arXiv:hep-ph/9707291v1 9 Jul 1997

LU/TP 97-14
UWThPh-1997-15
BUTP-97/17
HIP-1997-31 /TH

Pion–pion scattering at low energy

J. Bijnens[1], G. Colangelo[2], G. Ecker[3], J. Gasser[4] and M.E. Sainio[5]

[1] Dept. of Theor. Phys., Univ. Lund, Sölvegatan 14A, S–22362 Lund
[2] INFN – Laboratori Nazionali di Frascati, P.O. Box 13, I–00044 Frascati
[3] Inst. Theor. Phys., Univ. Wien, Boltzmanng. 5, A–1090 Wien
[4] Inst. Theor. Phys., Univ. Bern, Sidlerstr. 5, CH–3012 Bern
[5] Dept. of Physics, Univ. Helsinki, P.O. Box 9, FIN–00014 Helsinki

July 1997

Pacs: 11.30Rd, 12.39.Fe, 13.75.Lb
Keywords: Chiral Symmetry, Chiral Perturbation Theory, Pion–Pion Scattering

Abstract

We present technical details of the evaluation of the elastic $\pi\pi$ scattering amplitude to two loops in chiral perturbation theory. In particular, we elaborate on the renormalization procedure at the two–loop order and on the evaluation of the relevant Feynman diagrams that can all be expressed in terms of elementary functions. For the sake of clarity, we discuss these matters both in the N–component ϕ^4 theory (in its symmetric phase) and in chiral perturbation theory. Estimates for the relevant low–energy constants of $O(p^6)$ are presented. Threshold parameters and phase shifts are then calculated for two sets of $O(p^4)$ coupling constants and compared with experiment. We comment on the extraction of threshold parameters from phase shift data.

Contents

1 Introduction **2**

2 N–component ϕ^4 to two loops **3**
- 2.1 The loop expansion . . . 3
- 2.2 Renormalization . . . 5
  - 2.2.1 One–loop diagrams . . . 6
  - 2.2.2 Two–loop diagrams . . . 7
  - 2.2.3 The role of the equations of motion . . . 8
  - 2.2.4 Connection with the MS scheme . . . 10
- 2.3 Two– and four–point functions . . . 10
  - 2.3.1 Two–point function . . . 11
  - 2.3.2 Four–point function . . . 13

3 CHPT to two loops **16**
- 3.1 The lagrangian . . . 16
- 3.2 Renormalization at two–loop order . . . 19
  - 3.2.1 General analysis . . . 19
  - 3.2.2 Modified minimal subtraction . . . 21
  - 3.2.3 EOM and Laurent expansion of the coupling constants l_i . . . 22

4 Elastic $\pi\pi$ scattering to two loops **23**
- 4.1 Pion mass . . . 24
- 4.2 Pion decay constant . . . 25
- 4.3 The $\pi\pi$ scattering amplitude . . . 26

5 Numerical analysis **29**
- 5.1 Resonance saturation . . . 30
  - 5.1.1 Vector meson exchange . . . 30
  - 5.1.2 Scalar meson exchange . . . 31
  - 5.1.3 Kaon and eta contributions . . . 32
  - 5.1.4 Numerical values of the r_i . . . 32
- 5.2 The constants b_i . . . 33
- 5.3 Threshold parameters and phase shifts . . . 36

6 Conclusions **39**

A Fish and sunset diagrams **41**
A.1 Notation 41
A.2 The fish diagram 42
A.3 The sunset diagram 44

B Off–shell four–point function in d dimensions **46**

C Scattering lengths and effective ranges **47**

D The constants b_i **48**

References **50**

1 Introduction

Elastic $\pi\pi$ scattering is a fundamental process for QCD at low energies. It provides an ideal testing ground for the mechanism of spontaneous chiral symmetry breaking. Since only the (pseudo–)Goldstone bosons of chiral $SU(2)$ are involved, one expects the low–energy expansion of the scattering amplitude to converge rather rapidly. The systematic procedure for this low–energy expansion is called chiral perturbation theory (CHPT) [1, 2, 3, 4].

In the framework of CHPT, the $\pi\pi$ scattering amplitude was evaluated at lowest order in the chiral expansion in [5] and to next–to–leading order in [2, 6]. The theoretical developments up to 1994 are summarized in [7, 8]. The forthcoming experimental improvements concerning $\pi\pi$ scattering are also discussed there. The amplitude to next–to–next–to–leading order was recently calculated in a dispersive approach in [9] and in the standard CHPT framework in [10]. Other developments since 1994 can be found in Refs. [11]-[20].

Both the explicit calculation of the Feynman diagrams and the renormalization procedure needed to evaluate the scattering amplitude at the two–loop order are quite involved. The main aim of the present article is to detail the methods used in [10] for that purpose.

The amplitude contains a nontrivial analytical part that can be expressed in terms of logarithms that generate the cuts required by unitarity. In addition, there is a contribution which consists of a polynomial in the external momenta. Our calculation reveals the dependence of the six coefficients in this polynomial on the pion mass and on the low–energy constants of both $O(p^4)$ and $O(p^6)$. We find that the complete two–loop amplitude can be expressed in terms of elementary functions.

We found it useful to first illustrate in Sect. 2 the corresponding calculation in the N–component ϕ^4 theory (in its symmetric phase), where the algebraic manipulations needed are simple. The loop expansion is presented together with the renormalization at both the one– and two–loop levels. A technical issue that also comes up in the CHPT calculation is the use of the equations of motion (EOM) for the counterterms. We show how different forms of the counterterms at the one–

loop level lead to the same generating functional after a proper redefinition of the counterterms at the two–loop order.

In Sect. 3, the analogous calculation is performed in CHPT. The renormalization procedure is again discussed in detail, both for minimal subtraction and for the modified minimal subtraction that we actually use. For the effective chiral lagrangian, the role of EOM is similar as in ϕ^4, albeit algebraically more involved. In Sect. 4, the results for the pion mass, the pion decay constant and the $\pi\pi$ scattering amplitude are presented to $O(p^6)$ in the modified minimal subtraction scheme. Here, we also compare our results with the calculation of Ref. [9].

In Sect. 5, we perform a numerical analysis to compare with experimental information. For this purpose, we first derive estimates for the low–energy constants of $O(p^6)$. We include the effects of vector and scalar meson resonances and of K and η contributions. We then discuss numerically the sensitivity of the amplitude to those constants. We emphasize that the main uncertainties are due to the couplings of $O(p^4)$. We use two sets of these couplings to illustrate the uncertainty: The first set used in [10] is essentially based on phenomenology to $O(p^4)$ [2, 21]. For the second set, we use the present calculation to extract the couplings $\bar{l}_1$, $\bar{l}_2$ from the observed D–wave scattering lengths. For the two sets, we then analyse threshold parameters and phase shifts and compare them with available experimental results.

Sect. 6 contains our conclusions. Some technical aspects on the calculation of two–loop diagrams, the off–shell scattering amplitude of $O(p^4)$ and analytic expressions for the scattering lengths as well as for the coefficients b_i in the $O(p^6)$ amplitude are relegated to four appendices.

2 N–component ϕ^4 to two loops

As we have mentioned in the introduction, we illustrate the loop expansion in CHPT first with the N–component ϕ^4 theory in the unbroken phase. For this purpose, we proceed in a manner as analogous as possible to the chiral expansion. In particular, we rely on the external field technique and use a procedure that is scale independent at each step, as is done in CHPT. We also comment on the role of counterterms that vanish upon use of the EOM and give the relation to the MS scheme.

2.1 The loop expansion

The loop expansion is equivalent to an expansion of the generating functional in powers of $\hbar$ – we therefore explicitly display $\hbar$ in this section. The lagrangian is

$$\mathcal{L} \;=\; \frac{1}{2}(\partial_\mu\phi^T\partial^\mu\phi - M^2\phi^T\phi) - \frac{g}{4}(\phi^T\phi)^2 - \phi^T f - \sum_{\nu=1}^{\infty}\hbar^\nu C_\nu \;\;, \tag{2.1}$$

where the symbol ϕ collects the N fields $\phi_1,\ldots,\phi_N$,

$$\phi^T = (\phi_1,\ldots,\phi_N)\;.$$

Below, we will use an analogous notation for any multicomponent vector, e.g., $a^T = (a_1, a_2, a_3)$, etc. The quantities C_ν denote the counterterms that remove the

ultraviolet singularities at order $\hbar^\nu$. They are linear combinations of $O(N)$–invariant polynomials of dimension ≤ 4. Considering the external field f to be a spurion $O(N)$ vector and using partial integration to eliminate $\partial_\mu\phi^T\partial^\mu\phi$, one is left with

$$P_1 \;=\; \frac{1}{2}\phi^T\Box\phi \;\;,\; P_2 = \frac{1}{2}M^2\phi^T\phi \;\;,\; P_3 = \frac{g}{4}(\phi^T\phi)^2 \;\;,\; P_4 = \phi^T f \;. \tag{2.2}$$

As is shown below, one may eliminate one of these polynomials by use of the EOM. Here we discard P_4 and write

$$\begin{aligned} C_1 &= ga^T P \;\;,\; C_2 = g^2 b^T P \;\;,\; \ldots \;\;, \\ P^T &= (P_1, P_2, P_3) \;. \end{aligned} \tag{2.3}$$

In the following we use dimensional regularization. As a result, the vectors a and b become M–independent functions of the space–time dimension d, divergent as $d \to 4$. The external field f allows one to construct the generating functional by evaluating the vacuum–to–vacuum transition amplitude

$$\exp\{iZ[f]/\hbar\} = N\int[d\phi]\exp\{iS/\hbar\} \;\;,\; S = \int dx\,\mathcal{L} \;. \tag{2.4}$$

The normalization constant N ensures that $Z[0] = 0$. Expanding the right–hand side in powers of $\hbar$ generates the series

$$Z \;=\; Z_0 + \hbar Z_1 + \hbar^2 Z_2 + O(\hbar^3) \;.$$

To arrive at the explicit expressions for the components Z_i, one considers fluctuations around the classical solution $\bar\phi$ that is determined by the external field through the EOM,

$$(M^2 + \Box)\bar\phi^a + g\bar\phi^T\bar\phi\bar\phi^a + f^a = 0 \;\;;\;\; a = 1, \ldots, N \;. \tag{2.5}$$

Below, barred quantities always denote quantities evaluated at (2.5), e.g.,

$$\bar S = \int dx\,\mathcal{L}(\bar\phi[f], f) \;\;, \tag{2.6}$$

etc. We write the fluctuations in the form

$$\phi = \bar\phi + \xi \;\;, \tag{2.7}$$

use translation invariance of the measure, $[d\phi] = [d\xi]$, and find

$$\begin{aligned} \exp\{iZ/\hbar\} \;&=\; N\exp\{i\bar S/\hbar\}\times \\ &\qquad \int[d\xi]\exp\{\frac{-i}{\hbar}\int dx\,[\frac{1}{2}\xi^T D\xi + F(\xi,\bar\phi)]\} \;. \end{aligned} \tag{2.8}$$

The differential operator D acts in coordinate and flavour space,

$$\begin{aligned} D^{ab} &= D_0^{ab} + \sigma^{ab} \;\;, \\ D_0^{ab} &= (M^2 + \Box)\delta^{ab} \;\;,\; \sigma^{ab} = g\{\bar\phi^T\bar\phi\delta^{ab} + 2\bar\phi^a\bar\phi^b\} \;. \end{aligned} \tag{2.9}$$

Furthermore, considering the fluctuations to be of order $\hbar^{1/2}$, the quantity F starts at order $\hbar^{3/2}$. For the evaluation of the generating functional at two–loop order, it is sufficient to keep terms of order $\hbar^2$ in F,

$$\begin{aligned} F &= g\xi^T\xi\xi^T\bar{\phi} + \frac{g}{4}(\xi^T\xi)^2 + \hbar g\{\xi^T d_1\bar{\phi} + \xi^T d_2\xi\} + O(\hbar^{5/2}) \ , \\ d_1^{ab} &= (a_1\Box + a_2M^2 + a_3 g\bar{\phi}^T\bar{\phi})\delta^{ab} \ , \\ d_2^{ab} &= \frac{1}{2}\left(a_1\Box + a_2M^2\right)\delta^{ab} + \frac{a_3}{2}\sigma^{ab} \ . \end{aligned} \tag{2.10}$$

We then arrive at the following expressions for the components Z_i,

$$Z_0 = -\frac{1}{2}\int dx\,\left\{\overline{P}_4 - 2\overline{P}_3\right\} \ , \tag{2.11}$$

$$Z_1 = \frac{1}{2}\int dx\,\left\{i\langle\ln(1+D_0^{-1}\sigma)\rangle - 2\overline{C}_1\right\} \ , \tag{2.12}$$

$$Z_2 = -g^2\int dxdy\,\bar{\phi}_x^T\left\{2G_{xy}^3 + G_{xy}\langle G_{xy}^2\rangle\right\}\bar{\phi}_y \tag{2.13 a}$$

$$+\frac{g}{4}\int dx\,\left\{\left[\langle G_{xx}\rangle^2 + 2\langle G_{xx}^2\rangle\right] - [\cdots]_{\bar{\phi}=0}\right\} \tag{2.13 b}$$

$$-\frac{g^2}{2}\int dxdy\,\bar{\phi}_x^T\left\{\langle G_{xx}\rangle + 2G_{xx} + id_{1x}\right\}G_{xy}\times \left\{\langle G_{yy}\rangle + 2G_{yy} + id_{1y}\right\}\bar{\phi}_y \tag{2.13 c}$$

$$+ig\int dx\,\left\{\langle d_{2y}G_{yx}\rangle_{y=x} - \langle\cdots\rangle_{y=x,\bar{\phi}=0}\right\} \tag{2.13 d}$$

$$-\int dx\,\overline{C}_2 \ . \tag{2.13 e}$$

Here we have introduced the propagator in the presence of the external field f,

$$\begin{aligned} G_{xy} &= \int_0^\infty d\lambda\langle x|e^{-\lambda D}|y\rangle \ , \\ D_x^{ab}G_{xy}^{bc} &= \delta^{ac}\delta^{(d)}(x-y) \ . \end{aligned} \tag{2.14}$$

The symbol $\langle A\rangle$ denotes the trace of the matrix A in flavour space, and $\bar{\phi}_x = \bar{\phi}(x)$. The various contributions to Z_2 are illustrated in Fig. 1.

The numbering is such that the contribution (2.13 a) corresponds to Fig. 1a, etc. We refer in the following to Fig. 1a (b) as the sunset (butterfly) diagram, respectively. Below, we will also need the free propagator,

$$\triangle_{xy} = G_{xy}|_{f=0} \ , \tag{2.15}$$

which is a diagonal $N\times N$ matrix in flavour space.

2.2 Renormalization

The above expressions have a well–defined limit as the space–time dimension d reaches its physical value $d=4$ only for an appropriately chosen singular behaviour of the vectors a and b as $d\to 4$. In this subsection, we display and comment these singularities and start the discussion with the one–loop graphs.

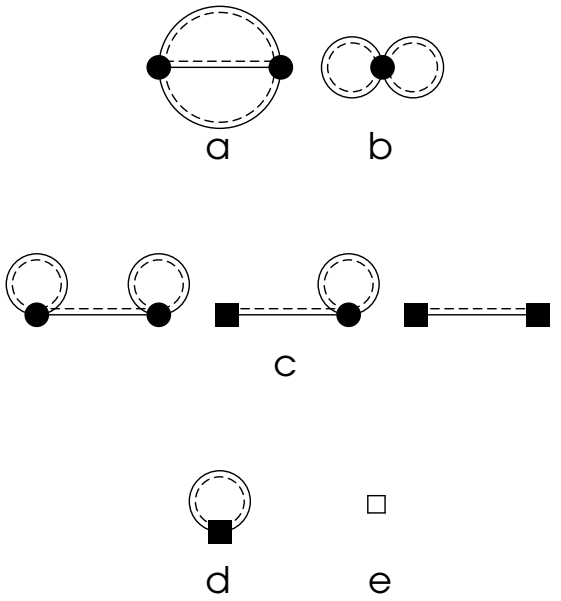

Figure 1: The two–loop graphs in ϕ^4 theory. Graph a corresponds to the contribution (2.13 a), and analogously for the diagrams b–e. The solid–dashed lines stand for the propagator (2.14). The black circles denote a vertex generated by the lagrangian $\mathcal{L}|_{C_i=0}$ in (2.1), and the filled squares stand for the contributions from the counterterm C_1. Finally, the contributions from the counterterm C_2 are indicated with an open square in graph e.

2.2.1 One–loop diagrams

The singularities at one–loop order may easily be identified by writing

$$\langle \ln(1 + D_0^{-1}\sigma)\rangle = \langle D_0^{-1}\sigma\rangle - \frac{1}{2}\langle D_0^{-1}\sigma D_0^{-1}\sigma\rangle + \cdots \quad ,$$

where the terms omitted are finite at $d = 4$. Evaluating the trace and keeping only the singular terms at $d = 4$ gives

$$i\int dx\,\langle \ln(1 + D_0^{-1}\sigma)\rangle = -g(N+2)T_M\int dx\,\bar{\phi}^T\bar{\phi} - \frac{g^2}{2}(N+8)\dot{T}_M\int dx\,(\bar{\phi}^T\bar{\phi})^2 + \cdots,$$

where the tadpole integral iT_M is the free propagator at coinciding arguments in coordinate space,

$$T_M = \frac{1}{i}\int_0^\infty d\lambda\langle x|e^{-\lambda D_0}|x\rangle = \frac{M^{d-2}}{(4\pi)^{d/2}}\Gamma(1-d/2) \quad , \tag{2.16}$$

and

$$\dot{T}_M \doteq \partial_{M^2}T_M = -\frac{M^{d-4}}{(4\pi)^{d/2}}\Gamma(2-d/2)\,. \tag{2.17}$$

To determine C_1, we work out the singular part in the integrals T_M and $\dot{T}_M$. We introduce the scale μ,

$$M^{2w} = \mu^{2w}(M/\mu)^{2w} \ , \ w = d/2 - 2 \ ,$$

and obtain

$$\begin{aligned} T_M &= \frac{M^2}{16\pi^2}\mu^{2w}\left\{\frac{1}{w} + a(M/\mu) - 1 + b(M/\mu)w + O(w^2)\right\} \ , \\ \dot{T}_M &= \frac{\mu^{2w}}{16\pi^2}\left\{\frac{1}{w} + a(M/\mu) + c(M/\mu)w + O(w^2)\right\} \ , \end{aligned} \tag{2.18}$$

with

$$a(M/\mu) = \ln(M^2/\mu^2) - \Gamma'(1) - \ln(4\pi) \ . \tag{2.19}$$

The functions $b(M/\mu)$ and $c(M/\mu)$ will not be needed in explicit form in the following. Since we have introduced the scale μ in such a manner that T_M and $\dot{T}_M$ are scale–independent, we may use scale–independent counterterms as well,

$$\begin{aligned} a_1 &= 0 \ , \\ a_2 &= \frac{\mu^{2w}}{16\pi^2}\left\{\frac{-(N+2)}{w} + a_2^r(\mu, w)\right\} \ , \\ a_3 &= \frac{\mu^{2w}}{16\pi^2}\left\{\frac{-(N+8)}{w} + a_3^r(\mu, w)\right\} \ , \end{aligned} \tag{2.20}$$

where the renormalized couplings $a_i^r(\mu, w)$ are finite at $w = 0$, with

$$\left(\mu\frac{\partial}{\partial\mu} + 2w\right) a_2^r(\mu, w) = 2(N+2) \ , \tag{2.21}$$

and analogously for a_3. With the choice (2.20, 2.21), the one–loop functional Z_1 is scale independent and finite at $d = 4$.

2.2.2 Two–loop diagrams

In the next step, we determine the counterterms that render the two–loop contributions finite at $d = 4$. For this purpose, we identify the singular part of the full propagator [22],

$$\begin{aligned} S_{xy} &= \triangle_{xy} + \sigma_x\dot{\triangle}_{xy} \ , \\ \dot{\triangle}_{xy} &= \partial_{M^2}\triangle_{xy} \ . \end{aligned}$$

The remainder R,

$$G_{xy} = S_{xy} + R_{xy} \ , \tag{2.22}$$

is finite at $x = y$. The decomposition (2.22) generates in the two–loop functional Z_2 terms of the form R^3, R^2S, RS^2 and S^3. A closer examination reveals that all nonlocal singularities proportional to R and to R^2 cancel out after putting in the values of the a_i from Eq. (2.20). The divergent contribution to Z_2 is therefore obtained by replacing everywhere in Z_2 the propagator G by its singular part, $G \to S$. We now sketch how the singular pieces are evaluated, and consider for illustration the part proportional to G^3_{xy} in Eq. (2.13 a) that contributes to the sunset diagram Fig. 1a. After $G \to S$, we expand the field $\bar{\phi}_y$ around $y = x$ and are then left with divergent vacuum integrals of the form

$$\int dx \left(\triangle^3_{xy};\, \triangle^2_{xy} \dot{\triangle}_{xy} \right) (1; (x-y)^\mu (x-y)^\nu) \ . \tag{2.23}$$

The integrals proportional to $\triangle^3_{xy}$ correspond to the sunset integrals H and $H^{\mu\nu}$ discussed in appendix A. The integrals that contain $\dot{\triangle}_{xy}$ can be evaluated in a similar manner. Proceeding in an analogous fashion for the remaining contributions to Z_2, we finally find that the following counterterms render the two–loop functional finite at $d = 4$:

$$\begin{aligned}
b_1 &= \left(\frac{\mu^{2w}}{16\pi^2}\right)^2 \left\{ \frac{(2+N)}{2w} + b_1^r(\mu, w) \right\} \ , \\
b_2 &= \left(\frac{\mu^{2w}}{16\pi^2}\right)^2 \left\{ \frac{(5+N)(2+N)}{w^2} + \frac{(2+N)}{w} \left(3 - a_2^r(\mu,w) - a_3^r(\mu,w)\right) + b_2^r(\mu,w) \right\} \ , \\
b_3 &= \left(\frac{\mu^{2w}}{16\pi^2}\right)^2 \left\{ \frac{(8+N)^2}{w^2} + \frac{2}{w} \left(22 + 5N - (8+N) a_3^r(\mu,w)\right) + b_3^r(\mu,w) \right\} \ .
\end{aligned} \tag{2.24}$$

Remark: In Eq. (2.24), the full contribution $a^r_{2,3}(\mu, w)$ to the singular part in $b_{2,3}$ occurs. We could have expanded $a^r_{2,3}(\mu, w)$ around $w = 0$ in (2.20) – then, only $a^r_{2,3}(\mu, 0)$ would occur in (2.24). In order to keep $a_{2,3}$ scale independent, additional terms of order $O(w)$ must then be added in (2.20). From (2.24) it is clear that these would contribute a local part to Z_2 that could then be removed with a redefinition of the renormalized couplings $b^r_i(\mu, w)$. The definition (2.20) allows one to do all this in one go.

2.2.3 The role of the equations of motion

We come back to the choice of the counterterms C_i[1]. In the generating functional, they are evaluated at the solution to the EOM. This amounts to a linear relation among the $\overline{P}_i$,

$$\begin{aligned}
E &\doteq 2P_1 + 2P_2 + 4P_3 + P_4 \ , \\
\overline{E} &= 0 \ .
\end{aligned} \tag{2.25}$$

[1] The following discussion is adapted to CHPT, where the higher–order lagrangians $\mathcal{L}_4, \mathcal{L}_6, \ldots$ take the role of the counterterms $C_1, C_2, \ldots$.

As we already mentioned, one may therefore remove one of the P_i from the list (2.2). We may e.g., eliminate P_3 instead of P_4 as above,

$$C_1 \to C_1' = g a'^T P' \ , \ P'^T = (P_1, P_2, P_4) \ . \tag{2.26}$$

Using the identity

$$\begin{aligned} a'^T P' &= c^T P + a_3' E \ , \\ c^T &= (a_1' - 2a_3', a_2' - 2a_3', -4a_3') \ , \end{aligned} \tag{2.27}$$

it is seen that a different choice of the counterterm at one–loop order amounts to adding to the lagrangian a term that vanishes at the solution to the EOM. As we now demonstrate, the use of C_1' requires that the counterterm at two–loop order must be adapted accordingly,

$$C_2 \ \to \ C_2' = g^2 b'^T P \ . \tag{2.28}$$

In C_2', we use again P – the freedom in the choice of polynomials occurs at each order in the perturbative expansion. We denote by Z_1', Z_2' the generating functional obtained with (2.26, 2.28). For the one–loop functional to be finite at $d = 4$, the integrals $\int dx\, \overline{C}_1'$ and $\int dx\, \overline{C}_1$ must have the same singularities. According to the relation (2.27), this requirement is satisfied with

$$a'^T = (-\frac{a_3}{2}, a_2 - \frac{a_3}{2}, -\frac{a_3}{4}) \ . \tag{2.29}$$

The replacement $C_1 \to C_1'$ then amounts to

$$C_1 \to C_1 + \kappa g E \ , \tag{2.30}$$

with $\kappa = -a_3/4$. This transformation obviously leaves the one–loop functional unchanged. Repeating the calculation of Z_2' with (2.30), one finds

$$Z_2' = Z_2 + \int dx \, \left(\overline{C}_2' - \overline{C}_2 \right) + \overline{Q} \ ,$$

where Q is a local action,

$$\begin{aligned} Q &= -g^2 \kappa \int dx e^T P \ , \\ e^T &= (2a_1 + \kappa, 2a_2 + \kappa, 4a_3 + 6\kappa) \ . \end{aligned} \tag{2.31}$$

In addition to the singularities in Z_2, the counterterm C_2' has to cancel the ones in $\overline{Q}$ as well. Because the latter is a local action, it can be removed from Z_2' altogether with

$$b' = b + \kappa e \ .$$

In summary, a different choice of the counterterm at one–loop order amounts to adding a term to the lagrangian that vanishes at the solution to the EOM, see Eq. (2.30). That transformation leaves Z_1 untouched and changes Z_2 by a local action $\overline{Q}$ which can be completely removed by an appropriate choice of the counterterm at two–loop order,

$$\left(\begin{array}{l} C_1 \to C_1 + \kappa g E \\ C_2 \to C_2 + g^2 e^T P \end{array} \right) \to Z_1' = Z_1, Z_2' = Z_2 \ . \tag{2.32}$$

2.2.4 Connection with the MS scheme

The above renormalization scheme generates scale–independent quantities at each step. In particular, individual Feynman diagrams are independent of μ. The Green functions so evaluated at one–loop accuracy contain the finite parameters $M^2, g, a_i(\mu,0), b_i(\mu,0), \ldots$ [2]. An analogous procedure is used in chiral perturbation theory [2]. We find it useful to compare at this stage this scheme with the MS scheme in conventional perturbative calculations. There, one starts from the bare lagrangian

$$\mathcal{L} = \frac{1}{2}(\partial_\mu \phi_B^T \partial^\mu \phi_B - M_B^2 \phi_B^T \phi_B) - \frac{g_B}{4}(\phi_B^T \phi_B)^2 \tag{2.33}$$

and sets at one–loop order

$$\begin{aligned} g_B &= \mu^{-2w} g_r(\mu) \left\{ 1 - \frac{(N+8)}{16\pi^2 w} g_r(\mu) + O(g_r^2) \right\} \ , \\ M_B^2 &= M_r^2(\mu) \left\{ 1 - \frac{(N+2)}{16\pi^2 w} g_r(\mu) + O(g_r^2) \right\} \ . \end{aligned} \tag{2.34}$$

The two schemes can easily be related by evaluating, e.g., the physical mass M_P and the elastic scattering amplitude to one–loop accuracy. This is done in the following subsection in the present scheme. Repeating that calculation with (2.33, 2.34) and identifying the one–loop expressions gives

$$\begin{aligned} g_r(\mu) &= g(1 + \frac{g a_3^r}{16\pi^2} + O(g^2)) \ , \\ M_r^2(\mu) &= M^2(1 + \frac{g a_2^r}{16\pi^2} + O(g^2)) \ . \end{aligned}$$

Here and in the following we use the notation

$$a_i^r \doteq a_i^r(\mu,0) \ , \ b_i^r \doteq b_i^r(\mu,0) \ .$$

From the scale dependence of the renormalized couplings a_2^r, a_3^r one reads off the scale dependence of M_r^2, g_r that guarantees scale independence of physical quantities. Analogous relations hold to all orders in the perturbative expansion.

2.3 Two– and four–point functions

For illustration, we evaluate the two–and four–point functions. It allows us to explain the methods used in Ref. [10] for the evaluation of the $\pi\pi$ scattering amplitude in CHPT.

[2] Of course, since the present theory is renormalizable, these parameters occur in such a combination that they can be lumped into, e.g., the physical mass M_P and the physical coupling constant.

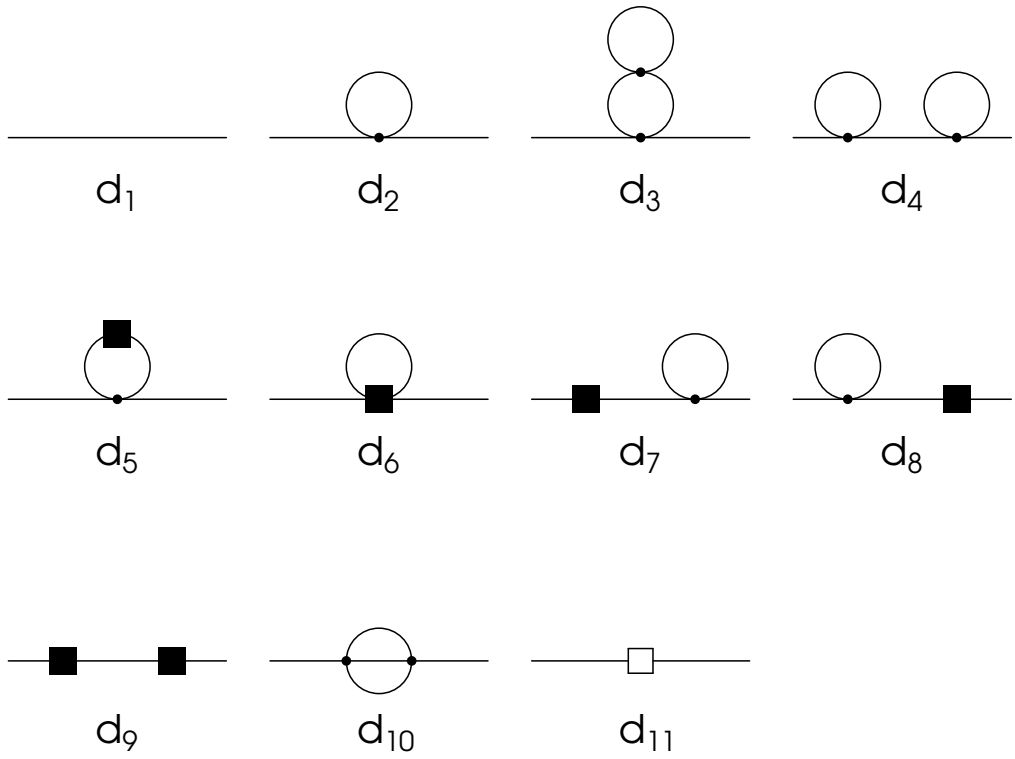

Figure 2: Diagrams that contribute to the two–point function at two–loop order. A filled square (open square) stands for the contributions from the counterterm $C_1(C_2)$.

2.3.1 Two–point function

To evaluate the two–point function

$$\begin{aligned} i\langle 0|T\phi^a(x)\phi^b(y)|0\rangle_{conn} &= \delta^{ab}\triangle'_{xy} \\ &= \delta^{ab}\left(N^{-1}\langle\triangle_{xy}\rangle + O(g)\right) \quad , \end{aligned} \tag{2.35}$$

we may either calculate the relevant Feynman diagrams displayed in Fig. 2, or determine the contribution of order f^2 to the generating functional, because

$$\delta^{ab}\triangle'_{xy} = \left.\frac{\delta^2 Z}{\delta f^a_x \delta f^b_y}\right|_{f=0} \quad . \tag{2.36}$$

We first proceed in this manner and find

$$\begin{aligned} Z &= \frac{1}{2}\int dx\, \bar{\phi}^T_x K_{xy}\bar{\phi}_y + O(\hbar^3, \bar{\phi}^4) \quad , \\ K_{xy} &= \delta^4(x-y)(A\Box_y + B) + C\triangle_{xy} + D\triangle^3_{xy} \end{aligned}$$

with

$$\begin{aligned} A &= 1 - g^2 b_1 \ , \\ B &= M^2 - g\, m^2 - g^2 \left\{ b_2 M^2 + (N+2)(a_3 T_M + m^2 \dot{T}_M) \right\} \ , \\ C &= g^2\, m^4 \ , \ D = -2g^2(N+2) \ , \\ m^2 &= a_2 M^2 + (N+2) T_M \ . \end{aligned} \tag{2.37}$$

Next we consider the Fourier transform

$$\begin{aligned} \triangle'(p^2) &= \int d^d x e^{-ip(x-y)} \triangle'_{xy} \\ &= \frac{1 - g^2 b_1}{M^2 - p^2 - B + M^2 A - 2g^2(N+2) H(p^2)} + O(g^3) \ , \end{aligned} \tag{2.38}$$

where $H(p^2)$ denotes the sunset integral (A.9). Expanding $H(p^2)$ around $p^2 = M^2$ gives at $d = 4$

$$\triangle'(p^2) = \frac{Z_\phi}{M_P^2 - p^2} + R_\phi(p^2) + O(g^3) \ , \tag{2.39}$$

with

$$Z_\phi = 1 + g^2 \frac{1}{(16\pi^2)^2} \left((N+2)(\frac{3}{4} + a(M/\mu)) - b_1^r \right) + O(g^3) \ , \tag{2.40}$$

and

$$R_\phi(p^2) = 2g^2(N+2) \overline{\overline{H}}(p^2) \ . \tag{2.41}$$

An integral representation for the twice subtracted sunset integral $\overline{\overline{H}}(p^2)$ – which is regular at $p^2 = M_P^2$ – is given in (A.12). Finally, the physical mass M_P can be easily evaluated from Eqs. (2.38, A.13) to two loops. The expansion starts with

$$\begin{aligned} M_P^2 &= M^2 + g m^2 + O(g^2) \\ &= M^2 \left\{ 1 + \frac{g}{16\pi^2} [(N+2)(a(M/\mu) - 1) + a_2^r] + O(g^2) \right\} \ . \end{aligned} \tag{2.42}$$

We add a remark concerning the calculation of the two–point function from the Feynman diagrams displayed in Fig. 2. Instead of evaluating the diagrams $\mathrm{d}_1, \ldots, \mathrm{d}_9$ individually, one may calculate the tree and tadpole graphs shown in Fig. 3, where the dashed and double lines stand for the propagators

$$\begin{aligned} \frac{1}{M_1^2 - p^2} \ , \ M_1^2 &= M^2[1 + g a_2 + g^2(b_2 - b_1)] \quad \text{(dashed line)} \\ \frac{1}{M_2^2 - p^2} \ , \ M_2^2 &= M^2 + g m^2 \quad \text{(double–line)} \end{aligned}$$

and where the vertex denotes the coupling $g(1 + a_3 g)$. The sum of these two diagrams is

$$\frac{1}{M_3^2 - p^2} \ , \qquad M_3^2 = M_1^2 + g(1 + a_3 g)(N+2) T_{M_2} \ , \tag{2.43}$$

where the argument in the tadpole integral is M_2. The expression (2.43) is equal to the sum of the graphs $\mathrm{d}_1, \ldots, \mathrm{d}_9$ up to terms beyond two loops.

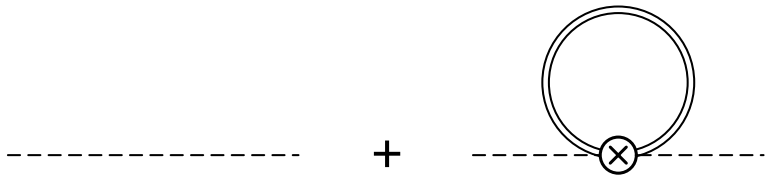

Figure 3: Summing up the graphs $\mathrm{d}_1 \cdots \mathrm{d}_9$ in Fig. 2. See text after Eq. (2.42).

2.3.2 Four–point function

The number of diagrams at two–loop order becomes quite large – of course even more so in the case of CHPT. In the case of the two–point function, we have just seen that almost all graphs in Fig. 2 can be summed up by evaluating the tadpole diagram shown in Fig. 3. Here we wish to illustrate an analogous method to evaluate the elastic scattering amplitude (four–point function) to two loops. Whereas the method does not really pay off in the case of the N–component ϕ^4 theory considered here, it turns out to be very useful in CHPT. Furthermore, a similar procedure works in the evaluation of form factors[3]. The four–point function is of the form

$$\begin{aligned} & i^3 \int dx_1\, dx_2\, dx_3\, e^{-i(p_1x_1+p_2x_2-p_3x_3-p_4x_4)} \langle 0|T\phi_i(x_1)\phi_k(x_2)\phi_l(x_3)\phi_m(x_4)|0\rangle \\ & = \frac{Z_\phi^2}{\prod_i (M_P^2 - p_i^2)} T_{lm;ik}(s,t,u;p_1^2,p_2^2,p_3^2,p_4^2) \quad , \end{aligned} \tag{2.44}$$

with

$$\begin{aligned} & p_1 + p_2 = p_3 + p_4 \quad , \\ & s = (p_1+p_2)^2 \quad , \; t = (p_1-p_3)^2 \quad , \; u = (p_1-p_4)^2 \; . \end{aligned}$$

The scattering amplitude is obtained by putting all momenta on the mass shell,

$$T_{lm;ik}(s,t,u;p_1^2,p_2^2,p_3^2,p_4^2)|_{p_i^2=M_P^2} = \delta_{ik}\delta_{lm} A(s,t,u) + \text{cycl.} \; .$$

To determine the amplitude $A(s,t,u)$, it suffices to calculate the matrix element for the indices

$$i = k = 1 \quad , \; m = l = N \; . \tag{2.45}$$

The relevant graphs up to $O(g^3)$ are displayed in Fig. 4. The numbers attached on the external lines denote the relevant momenta, $i \leftrightarrow p_i$. The group indices and crossed diagrams are not shown, and mass and counterterm insertions on the external lines are not displayed.

We use the obvious notation

$$A(s,t,u) = gA^{(1)} + g^2 A^{(2)} + g^3 A^{(3)} + O(g^4) \; . \tag{2.46}$$

[3]This method has already been used in [23, 24] in connection with the evaluation of the process $\gamma\gamma \to \pi\pi$ to two loops.

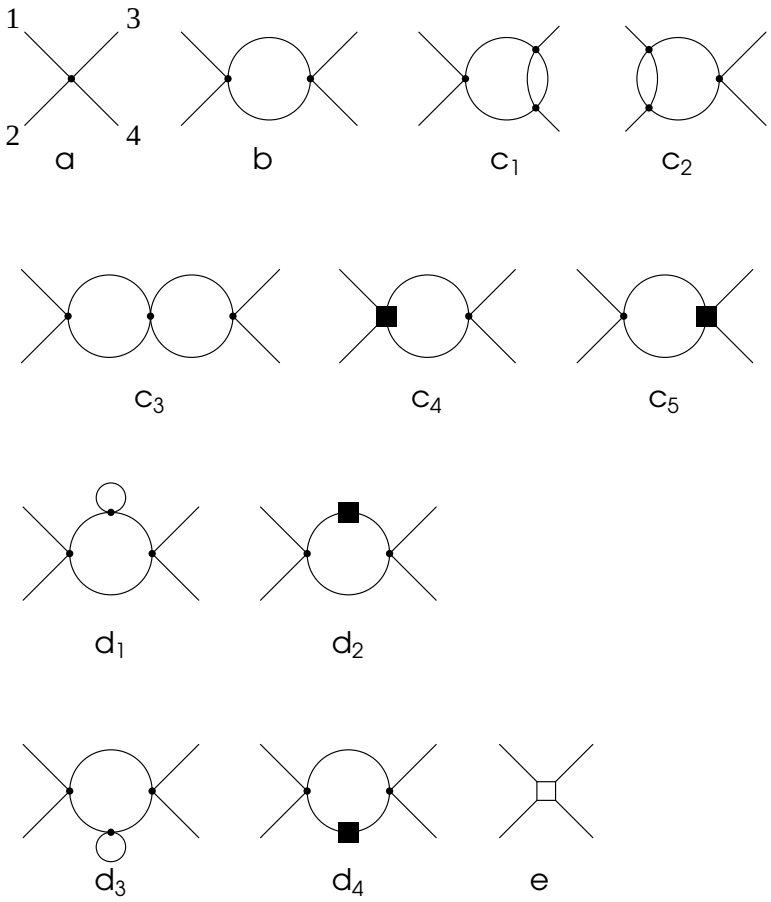

Figure 4: The elastic $\phi\phi \to \phi\phi$ scattering amplitude to two loops. The numbers on the external lines denote the momenta. Crossed diagrams and insertions on external lines are not displayed. A filled box (open box) denotes contributions from the counterterm $C_1(C_2)$.

The tree–level and one–loop results are

$$\begin{aligned} A^{(1)}(s,t,u) &= -2 \ , \\ A^{(2)}(s,t,u) &= -\frac{2}{16\pi^2}\left[a_3^r + (N+8)a(M/\mu)\right] \\ &+ 2(N+4)\bar{J}(s) + 4\left[\bar{J}(t)+\bar{J}(u)\right] \ , \end{aligned} \tag{2.47}$$

with

$$\bar{J}(z)=\frac{1}{16\pi^2}\left[\sigma \ln\frac{\sigma-1}{\sigma+1}+2\right] \quad ; \quad \sigma = \left(1-4M^2/z\right)^{\frac{1}{2}} \ . \tag{2.48}$$

The calculation at two–loop order may be made more economical by using the renormalized one–loop off–shell amplitude as a single (nonlocal) vertex. Then, a

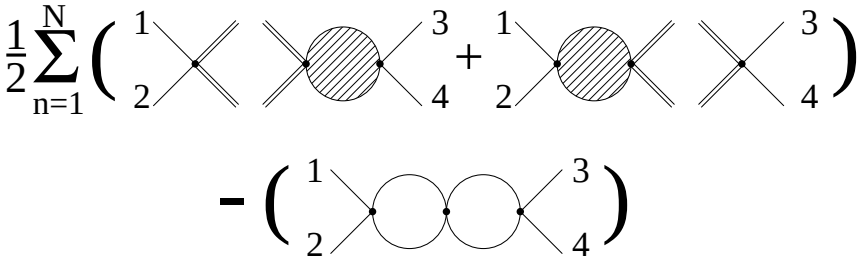

Figure 5: Summing up the diagrams $c_1 \cdots c_5$ in Fig. 4. See text after Eq. (2.47).

large part of the two–loop diagrams can be obtained automatically by making a one–loop calculation where one of the vertices is the one–loop amplitude, and the other is the standard tree–level vertex. To be more specific, consider the diagrams Fig. 4c_1,...,c_5. They can be calculated by evaluating the integrals indicated in Fig. 5. The notation is as follows: The double lines denote off–shell legs (the corresponding off–shell amplitude is defined in (2.44)). These legs carry momenta l and $(p_1 + p_2 - l)$, and group index n. The integration has to be done with weight

$$\frac{1}{(M^2 - l^2)(M^2 - (p_1 + p_2 - l)^2)} \; .$$

From this sum, one has to subtract the diagram Fig. 4c_3. The result equals the diagrams Fig. 4c_1,...,c_5.

One may easily check the correctness of this statement, if one singles out of the full one–loop amplitude one particular diagram. In this manner one generates a single two–loop diagram with a symmetry factor in front of it: One can then compare this to what one would get from a standard Feynman diagram calculation. Similar formulae hold, of course, for the crossed versions of these diagrams.

After checking that the method is correct, the second question to be answered is how one can do Feynman loop integrals with a nonlocal vertex in it. In particular, how does one perform the following integral:

$$\int \frac{d^d l}{(2\pi)^d} \frac{\bar{J}((l - p_3)^2)}{(M^2 - l^2)(M^2 - (p_1 + p_2 - l)^2)} \; . \tag{2.49}$$

First we remark that this integral has to be calculated anyway, even if one would try to calculate directly the two–loop diagrams. It corresponds to the fish diagram in Fig. 4c_1, where the divergence of the one–loop subdiagram has already been cancelled by the insertion of the counterterm Fig. 4c_5. As can be seen here, one of the advantages of the method is that one starts the calculation at a stage where the one–loop subdivergence has already been subtracted.[4] This fact is of relevance in particular in CHPT, where one may thus first do the renormalization of the off–shell one-loop amplitude before diving into the forest of two–loop integrals. Next we

[4]The subtraction of the subdivergence in the diagram Fig. 4c_3 is much easier to accomplish, because the corresponding integral is a product of two one–loop integrals.

note that the loop function $\bar{J}(s)$ admits a dispersive representation in d dimensions [23, 24]:

$$\bar{J}(t) = t \int_{4M^2}^{\infty} \frac{[dx]}{x(x-t)} \ , \tag{2.50}$$

where the measure $[dx]$ is given in appendix A (for $M^2 = 1$). By inserting this expression into Eq. (2.49) we see that the problem is transformed into the calculation of a one–loop integral with three propagators, where one of the propagators has a variable mass over which we finally have to integrate:

$$\int_{4M^2}^{\infty} \frac{[dx]}{x} \int \frac{d^d l}{(2\pi)^d} \frac{(l-p_3)^2}{(M^2-l^2)(M^2-(l-p_3-p_4)^2)(x-(l-p_3)^2)} \ . \tag{2.51}$$

We discuss in appendix A how this integral can be done explicitly [30].

Finally, we are left with the graphs that we have not yet taken into account: The tadpole and counterterm insertions displayed in Fig. $4\mathrm{d}_{1,\ldots,4}$ can easily be taken care of by simply replacing in the one–loop integrals the parameter M with the physical mass M_P. The contributions from wave function renormalization is taken care of by multiplying the tree graph with Z_ϕ^2.

In summary, the advantages of the approach just described are that i) by using the renormalized one–loop amplitude as a single nonlocal vertex, the divergences due to one–loop subgraphs in nonfactorizable integrals never appear; ii) the diagrams that produce the mass renormalization inside the one–loop amplitude are taken into account trivially and do not have to be calculated explicitly; iii) the method also applies to the calculation of form factors, or any process where one part is given by an elastic two–body process like $\gamma\gamma \to \pi\pi$ [23]; iv) the method can easily be implemented into a computer algebra program like FORM [25].

3 CHPT to two loops

In the following we discuss the methods used in Ref. [10] to evaluate the elastic $\pi\pi$ scattering amplitude to two loops in the framework of CHPT. This section contains details concerning renormalization, whereas the two–loop expressions for the pion mass, the pion decay constant and the scattering amplitude are given in the following section.

3.1 The lagrangian

The effective lagrangian consists of a string of terms,

$$\mathcal{L}_{\text{eff}} = \mathcal{L}_2 + \hbar\mathcal{L}_4 + \hbar^2\mathcal{L}_6 + \ldots . \tag{3.1}$$

Depending on the application one has in mind, one has to keep external fields in $\mathcal{L}_{\text{eff}}$. In the present case, we wish to calculate M_π, F_π and the $\pi\pi$ scattering amplitude. The pion mass and the scattering amplitude may both be calculated from on–shell

quantities, and external fields are thus not necessary. On the other hand, the pion decay constant needs a weak current as an external probe – it is an off–shell quantity, not accessible through on–shell matrix elements. The use of the axial current to evaluate F_π to two loops is cumbersome because of the presence of Lorentz indices. In the following, we use instead the two–point function of pseudoscalar densities. A Ward identity relates the residue of this quantity to the pion decay constant.

There are many choices for the pion fields to be used in the effective lagrangians. Of course, the result for physical quantities is always the same. A convenient choice to minimize the number of diagrams is the sigma model parametrization. In the following we work in the isospin symmetry limit $m_u = m_d$. We have

$$\mathcal{L}_2 = \frac{F^2}{4} \langle u_\mu u^\mu + \chi_+ \rangle \quad , \tag{3.2}$$

with

$$\begin{aligned} U &= \sigma + i\frac{\boldsymbol{\phi}}{F} \ , \ \sigma^2 + \frac{\boldsymbol{\phi}^2}{F^2} = \mathbf{1} \ , \\ \boldsymbol{\phi} &= \begin{pmatrix} \pi^0 & \sqrt{2}\pi^+ \\ \sqrt{2}\pi^- & -\pi^0 \end{pmatrix} = \phi^i \tau^i \ , \\ u_\mu &= i u^\dagger \partial_\mu U u^\dagger = -i u \partial_\mu U^\dagger u = u_\mu^\dagger \ , \\ \chi_+ &= u^\dagger \chi u^\dagger + u \chi^\dagger u \ , \\ \chi &= 2B(\hat{m}\mathbf{1} + ip) \ , \ \hat{m} = \frac{1}{2}(m_u + m_d) \ , \end{aligned} \tag{3.3}$$

with $u^2 = U$. Furthermore, $p = p^i \tau^i$ is the external pseudoscalar field referred to above. The symbol $\langle A \rangle$ denotes the trace of the two–by–two matrix A. The lagrangian $\mathcal{L}_4$ is [2]

$$\mathcal{L}_4 = \sum_{i=1}^{4} l_i P_i + \dots \quad , \tag{3.4}$$

where

$$P_1 = \frac{1}{4}\langle u^\mu u_\mu \rangle^2 \ , \ P_2 = \frac{1}{4}\langle u_\mu u_\nu \rangle \langle u^\mu u^\nu \rangle \ , \ P_3 = \frac{1}{16}\langle \chi_+ \rangle^2 \ , \ P_4 = \frac{i}{4}\langle u_\mu \chi_-^\mu \rangle \ , \tag{3.5}$$

with

$$\chi_-^\mu = u^\dagger \partial^\mu \chi u^\dagger - u \partial^\mu \chi^\dagger u \ . \tag{3.6}$$

The ellipsis in Eq. (3.4) denotes terms that do not contribute to the quantities considered here. The low–energy constants l_i are divergent and remove the ultraviolet divergences generated by one–loop graphs from $\mathcal{L}_2$. We discuss them in more detail below.

The complete effective lagrangian $\mathcal{L}_6$ is not yet available: Whereas the list of the necessary counterterms has been published [26], their divergence structure at $d = 4$ is

still under investigation [27]. The knowledge of these would provide us with a check on the calculation, because these divergences must cancel the ones that we find in the two–loop calculation. Apart from this check, however, that analysis would not be of further use in the present context, because the scale–dependent finite pieces of those couplings are still largely unknown. Nevertheless, the structure displayed in [26] shows that there are no algebraic constraints between the counterterms at $O(p^6)$ needed in the expressions for the pion mass, pion decay constant or $\pi\pi$ scattering amplitude.

For the following considerations, it is useful to recall that the expansion in powers of the momenta is equivalent to an expansion in inverse powers of F^2. In an obvious notation, the chiral expansion for the pion mass, the pion decay constant and the elastic $\pi\pi$ scattering amplitude is

$$\begin{aligned} M_\pi^2 &= M^2 \left\{ 1 + m_4 \frac{M^2}{F^2} + m_6 \frac{M^4}{F^4} + O(F^{-6}) \right\} \ , \\ F_\pi &= F \left\{ 1 + f_4 \frac{M^2}{F^2} + f_6 \frac{M^4}{F^4} + O(F^{-6}) \right\} \ , \\ A(s,t,u) &= \frac{A_2}{F^2} + \frac{A_4}{F^4} + \frac{A_6}{F^6} + O(F^{-8}) \ . \end{aligned} \tag{3.7}$$

The one–loop contributions m_4, f_4 and A_4 have been determined in [6] – here, we calculate m_6, f_6 and A_6. Therefore, we need to keep in the effective lagrangian only contributions up to $O(F^{-6})$. We write symbolically

$$\begin{aligned} \mathcal{L}_2 &= \mathcal{L}_{kin} + a_1 \frac{\boldsymbol{\phi}^4}{F^2} + a_2 \frac{\boldsymbol{\phi}^6}{F^4} + a_3 \frac{\boldsymbol{\phi}^8}{F^6} + O(F^{-8}) \ , \\ \mathcal{L}_4 &= b_1 \frac{\boldsymbol{\phi}^2}{F^2} + b_2 \frac{\boldsymbol{\phi}^4}{F^4} + b_3 \frac{\boldsymbol{\phi}^6}{F^6} + O(F^{-8}) \ , \\ \mathcal{L}_6 &= c_2 \frac{\boldsymbol{\phi}^2}{F^4} + c_3 \frac{\boldsymbol{\phi}^4}{F^6} + O(F^{-8}) \ , \end{aligned} \tag{3.8}$$

where the dimension of the couplings is

$$[a_i] = \text{mass}^2 \ , \ [b_i] = \text{mass}^4 \ , \ [c_i] = \text{mass}^6 \ . \tag{3.9}$$

In order to generate a term of order F^{-2m}, one has to consider all products

$$a_{n_1}^{m_1} b_{n_2}^{m_2} c_{n_3}^{m_3} \quad ; \quad m_1 n_1 + m_2 n_2 + m_3 n_3 = m \ . \tag{3.10}$$

Furthermore, it is very convenient to collect the terms quadratic in the pion fields in the kinetic part and to expand in powers of b_1 and c_2 only afterwards. As a result, one has to consider the following products:

$$\begin{aligned} m_6, f_6 : &\quad a_1^2; \quad a_2; \quad b_2 \\ A_6 : &\quad a_1^3; \quad a_1 a_2; \quad a_3; \quad a_1 b_2; \quad b_3; \quad c_3 \ . \end{aligned} \tag{3.11}$$

3.2 Renormalization at two–loop order

3.2.1 General analysis

The loop contributions to M_π, F_π and to the scattering amplitude $A(s,t,u)$ are divergent in the limit $d \to 4$. Using the notation (3.7), we are concerned here with the renormalization of the quantities m_6, f_6 and A_6. As is guaranteed by general theorems of renormalization theory [28], the divergent parts of m_6 and f_6 are mass independent in dimensional regularization. Likewise, the divergent part of A_6 is a polynomial in the external momenta and in M^2. The most general crossing symmetric polynomial arising at order p^6 is

$$\begin{aligned} F^6 A_6^{\rm pol} &= A^{(1)} M^6 + A^{(2)} s M^4 + A^{(3)} s^2 M^2 + A^{(4)} (t-u)^2 M^2 \\ &\quad + A^{(5)} s^3 + A^{(6)} s (t-u)^2 \end{aligned}$$

with six coefficients $A^{(1)}, \ldots, A^{(6)}$. Like m_6 and f_6, they receive contributions from two–loop graphs with $\mathcal{L}_2$, one–loop graphs with one vertex from $\mathcal{L}_4$ and tree graphs generated by $\mathcal{L}_2 + \mathcal{L}_4 + \mathcal{L}_6$, see Eq. (3.11). The following analysis applies to each of the eight coefficients $m_6, f_6, A^{(1)}, \ldots, A^{(6)}$ separately. Denoting these coefficients generically as Q, we write

$$Q = Q_{\rm loop} + Q_{\rm tree} \ . \tag{3.12}$$

Since Q is part of a measurable quantity, it must of course be finite (and scale independent). The two components $Q_{\rm loop}$ and $Q_{\rm tree}$, on the other hand, are both divergent. Concentrating first on $Q_{\rm loop}$, dimensional regularization produces for m_6 and f_6 the general form

$$Q_{\rm loop} = \dot{T}_M \left\{ \dot{T}_M x(d) - \sum_{i=1}^{4} l_i(d) y_i(d) \right\} \ , \tag{3.13}$$

where $x(d), y_i(d)$ are dimensionless functions of d, finite at $d = 4$. (For the sake of clarity, we exhibit in this section the dependence of the low–energy couplings $l_i(d)$ on the space–time dimension d.) The same structure is found for the six coefficients $A^{(i)}$. We perform a Taylor series expansion,

$$\begin{aligned} x(d) &= x_0 + x_1 w + x_2 w^2 + O(w^3) \ , \\ y_i(d) &= y_{i0} + y_{i1} w + y_{i2} w^2 + O(w^3) \quad ; i = 1, \ldots, 4 \ ; \ w = \frac{d}{2} - 2 \end{aligned}$$

with real numbers $x_0, x_1, x_2, y_{i0}, y_{i1}, y_{i2}$. The tadpole integral $\dot{T}_M$ (2.17) and the low–energy constants $l_i(d)$ are both divergent as $w \to 0$. The Laurent expansion of the tadpole integral is displayed in (2.18). For the low–energy constants $l_i(d)$, we write

$$\begin{aligned} l_i(d) &= \frac{\mu^{2w}}{(4\pi)^2} \left[\frac{\gamma_i}{2w} + l_{i,r}^{\rm MS}(\mu, w) \right] \ , \\ \gamma_1 &= \frac{1}{3} \ , \ \gamma_2 = \frac{2}{3} \ , \ \gamma_3 = -\frac{1}{2} \ , \ \gamma_4 = 2 \ . \end{aligned} \tag{3.14}$$

For reasons already explained in Sect. 2 in the framework of the N–component ϕ^4 theory, we have not expanded the renormalized couplings $l_{i,r}^{\rm MS}(\mu, w)$ around $w = 0$. See comments after Eq. (2.24) and the discussion below.

Since there must not be any terms of the form

$$\frac{\ln M/\mu}{w}$$

in $Q_{\rm loop}$, there are eight consistency conditions (for each of the eight coefficients $m_6, f_6, A^{(i)}$) of the type [1]

$$x_0 = \frac{1}{4}\sum_{i=1}^{4} \gamma_i y_{i0} \ . \tag{3.15}$$

This absence of mass singularities in the divergences provides an extra check on our calculation. Using the equality (3.15) that relates one– and two–loop parameters, one gets (from now on, the summation convention is implied for $i = 1, \ldots, 4$)

$$\begin{aligned}
Q_{\rm loop} &= \frac{\mu^{4w}}{(4\pi)^4}\left\{\frac{Q_2}{w^2} + \frac{Q_1}{w} + Q_0 + O(w)\right\} \ , \\
Q_2 &= -x_0 \ , \ Q_1 = x_1 - l_{i,r}^{\rm MS}(\mu, w) y_{i0} - \frac{1}{2}\gamma_i y_{i1} \ , \\
Q_0 &= x_0 a(M/\mu)^2 + \left[2x_1 - l_{i,r}^{\rm MS}(\mu) y_{i0} - \frac{1}{2}\gamma_i y_{i1}\right] a(M/\mu) \\
&\quad + x_2 - l_{i,r}^{\rm MS}(\mu) y_{i1} - \frac{1}{2}\gamma_i y_{i2} \ ,
\end{aligned}$$

where

$$l_{i,r}^{\rm MS}(\mu) \doteq l_{i,r}^{\rm MS}(\mu, 0) \ .$$

It is seen that the coefficient $c(M/\mu)$ in the Laurent expansion (2.18) of the tadpole integral $\dot{T}_M$ does not enter due to the relation (3.15).

The pole terms can now be absorbed by the tree–level contribution $Q_{\rm tree}$ which is a certain combination (depending on the specific observable under consideration) of coupling constants in the general chiral lagrangian $\mathcal{L}_6$. Denoting this combination generically as $z(d)$, the expansion analogous to (3.14) is

$$Q_{\rm tree}(d) \doteq z(d) = \frac{\mu^{4w}}{(4\pi)^4}\left\{-\frac{Q_2}{w^2} - \frac{Q_1}{w} + (4\pi)^4 z_r^{\rm MS}(\mu) + O(w)\right\} \ . \tag{3.16}$$

The sum $Q_{\rm loop} + Q_{\rm tree}$ is finite and independent of the scale μ by construction. Taking the limit $d \to 4$ yields

$$\lim_{d\to 4} Q = \frac{Q_0}{(4\pi)^4} + z_r^{\rm MS}(\mu) \ . \tag{3.17}$$

Recalling the scale independence of $Q, \dot{T}_M, l_i(d)$ and of $z(d)$, one derives the renormalization group equation for the renormalized coupling constant $z_r^{\rm MS}$:

$$\mu \frac{dz_r^{\rm MS}(\mu)}{d\mu} = \frac{2}{(4\pi)^4} \left[2x_1 - l_{i,r}^{\rm MS}(\mu) y_{i0} - \gamma_i y_{i1} \right] \ . \tag{3.18}$$

Comparing Eqs. (2.19), (3.15) and (3.17), we recover the well–known fact [1, 23, 19] that the coefficient of the double logs can be determined solely from one–loop diagrams with a single vertex from $\mathcal{L}_4$.

3.2.2 Modified minimal subtraction

The above renormalization procedure corresponds to minimal subtraction, where powers of $\ln 4\pi + \Gamma'(1)$ occur in the final expressions, see (2.19). These terms can be absorbed by splitting from the renormalized couplings $l_{i,r}^{\rm MS}(\mu)$ and $z_r^{\rm MS}(\mu)$ appropriate finite pieces [29]. The procedure is based on the relation

$$\frac{\Gamma(1-w)}{(4\pi)^w} \exp w[\Gamma'(1) + \ln 4\pi] = \exp \sum_{n=2}^{\infty} \frac{\zeta(n)}{n} w^n \ , \tag{3.19}$$

which shows that a simple factor is responsible for these terms. To remove them, one pulls out a factor c^{2w} in the definition of the renormalized couplings in (3.14),

$$l_i(d) \ = \ \frac{(\mu c)^{2w}}{(4\pi)^2} \left\{ \frac{\gamma_i}{2w} + l_{i,r}^c(\mu, w) \right\} \ , \tag{3.20}$$

as a result of which $Q_{\rm loop}$ in (3.13) becomes

$$Q_{\rm loop} = (\mu c)^{4w} \left\{ (\mu c)^{-4w} \dot{T}_M^2 \, x(d) - (\mu c)^{-2w} \frac{\dot{T}_M}{(4\pi)^2} \sum_{i=1}^{4} \left[\frac{\gamma_i}{2w} + l_{i,r}^c(\mu, w) \right] y_i(d) \right\}. \tag{3.21}$$

Pulling out in the analogous manner c^{4w} in Eq. (3.16),

$$z(d) = \frac{(\mu c)^{4w}}{(4\pi)^4} \left\{ \cdots + (4\pi)^4 z_r^c(\mu) \right\} \ , \tag{3.22}$$

shows that these redefinitions amount to the change

$$\begin{aligned} \ln \frac{M}{\mu} &\to \ln \frac{M}{\mu} - \ln c \ , \\ \left(l_{i,r}^{\rm MS}(\mu), z_r^{\rm MS}(\mu) \right) &\to \left(l_{i,r}^c(\mu, 0), z_r^c(\mu) \right) \ , \end{aligned} \tag{3.23}$$

in Eq. (3.17).

The traditional choice for c in CHPT is [2]

$$\ln c = -\frac{1}{2} \left[\ln 4\pi + \Gamma'(1) + 1 \right] \ .$$

In this scheme, one uses the notation [2]

$$l_i(d) = l_i^r(\mu) + \frac{\mu^{2w}\gamma_i}{(4\pi)^2}\left\{\frac{1}{2w} - \frac{1}{2}[\ln 4\pi + \Gamma'(1) + 1]\right\} + O(w) \ ,$$

where

$$l_i^r(\mu) = \frac{1}{(4\pi)^2} l_{i,r}^c(\mu, 0)$$

according to (3.20). Similarly, we write

$$z^r(\mu) \doteq z_r^c(\mu) \tag{3.24}$$

for the above choice of the constant c.

We have thus arrived at the final expressions that will be used for M_π, F_π and $A(s,t,u)$:

$$\begin{aligned} Q &= \frac{1}{(4\pi)^4}\left\{x_0\left[1 + 2\ln\frac{M}{\mu}\right]^2 + \left[2x_1 - \frac{1}{2}\gamma_i y_{i1} - (4\pi)^2 l_i^r(\mu) y_{i0}\right]\left(1 + 2\ln\frac{M}{\mu}\right)\right. \\ &\quad \left. + x_2 - \frac{1}{2}\gamma_i y_{i2} - (4\pi)^2 l_i^r(\mu) y_{i1} + (4\pi)^4 z^r(\mu)\right\} \ . \end{aligned} \tag{3.25}$$

The scale dependence of the renormalized couplings is

$$\begin{aligned} \mu\frac{dz^r(\mu)}{d\mu} &= \frac{2}{(4\pi)^4}[2x_1 - (4\pi)^2 l_i^r(\mu) y_{i0} - \gamma_i y_{i1}] \ , \\ \mu\frac{dl_i^r(\mu)}{d\mu} &= -\frac{\gamma_i}{(4\pi)^2} \ . \end{aligned}$$

3.2.3 EOM and Laurent expansion of the coupling constants l_i

We include here a brief discussion of some technical aspects of the renormalization program at $O(p^6)$. In Sect. 2, it was shown that the counterterms of ϕ^4 theory can be written in different forms using the EOM. Transforming from one set of counterterms to another leaves the functional Z_1 unchanged and produces an additional local action of $O(\hbar^2)$ that can always be absorbed by changing the coefficients of the counterterms in Z_2.

The situation in CHPT is similar. Using the EOM of CHPT, both the lagrangians of $O(p^4)$ and $O(p^6)$ can take different forms. Since to $O(p^6)$ the lagrangian $\mathcal{L}_6$ enters only at the classical solution, such a modification has no effect at all as far as $\mathcal{L}_6$ is concerned. The same is true for all quantities of $O(p^4)$. However, the couplings in the lagrangian $\mathcal{L}_4$ also appear in one–loop and tree diagrams contributing at $O(p^6)$. In this case, different forms of $\mathcal{L}_4$ lead to different results a priori.

As for the ϕ^4 theory in Sect. 2, the natural place to discuss those modifications is the generating functional of Green functions. Referring to a forthcoming paper [27] for an explicit proof, we present here only the final result. Lagrangians of $O(p^4)$

that differ by the EOM lead to generating functionals that differ by local actions of $O(p^6)$. Since those actions are of course chirally symmetric they can always be absorbed by a redefinition of the low–energy constants of $O(p^6)$.

If the low–energy constants are determined phenomenologically by comparison with experiment, the result is of course independent of the form of $\mathcal{L}_4$. On the other hand, using a model for the constants of $O(p^6)$ like resonance saturation does not specify the form of $\mathcal{L}_4$. Therefore, different forms of $\mathcal{L}_4$ lead to different numerical results because the constants of $O(p^6)$ are by definition unchanged. For the $\pi\pi$ scattering amplitude, it turns out that the coefficients $b_1,\ldots,b_4$ are affected by this ambiguity while b_5 and b_6 are not modified. We come back in Sect. 5 to a numerical discussion of this ambiguity.

The second issue we want to address is the dependence of the low–energy constants l_i of $O(p^4)$ on the dimension of space–time. In Eq. (3.14), we have defined functions $l_{i,r}^{\rm MS}(\mu,w)$ that contain all non–singular pieces of the $l_i(d)$. These functions enter in the quantity Q_1 in $Q_{\rm loop}$ and they are subtracted by the appropriate decomposition of $Q_{\rm tree}$ in (3.16). As a consequence, only the coefficients $l_{i,r}^{\rm MS}(\mu) \doteq l_{i,r}^{\rm MS}(\mu,0)$ appear in renormalized quantities.

Although this is a completely legal subtraction procedure, it is by no means obvious that this procedure can be applied consistently for all possible processes. In other words, the question is whether the low–energy constants of $O(p^6)$ can be decomposed as in Eq. (3.16) in a process–independent way such that only the $l_{i,r}^{\rm MS}(\mu)$ appear in all observable quantities. To discuss this issue for the case of minimal subtraction, we expand the $l_i(d)$ up to first order in w:

$$l_i(d) = \frac{\mu^{2w}}{(4\pi)^2}\left[\frac{\gamma_i}{2w} + l_{i,r}^{\rm MS}(\mu) + \delta_i(\mu)w + O(w^2)\right]. \tag{3.26}$$

The terms of $O(w^2)$ cannot contribute to $O(p^6)$ because the l_i appear only in diagrams that are not more singular than $1/w$ (except for the divergent parts of the l_i themselves). However, the coefficients $\delta_i(\mu)$ certainly do appear at $O(p^6)$. The subtraction procedure (3.16) leads to the following two questions:

- Do the coefficients $\delta_i(\mu)$ appear always in local contributions of $O(p^6)$ only?
- If yes, can they be absorbed into the coupling constants of $O(p^6)$ in a process–independent manner?

The crucial question is of course the first one. It can be shown [31, 27] that the terms involving the δ_i indeed take the form of local actions in the generating functional of $O(p^6)$, see also the analogous discussion in the framework of the N–component ϕ^4 theory in Sect. 2. Although these contributions depend on the choice of the lagrangian of $O(p^4)$ (EOM), they can therefore always be absorbed in the low–energy constants of $O(p^6)$ in a process–independent way. Thus, the subtraction procedure (3.16) is a special case of a general method. It has already been used in [23, 24, 33].

4 Elastic $\pi\pi$ scattering to two loops

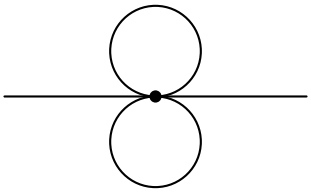

Figure 6: Butterfly diagram contribution to the two–point function (4.1).

4.1 Pion mass

We consider the connected two–point function

$$\triangle^{ik}(p^2) = i \int d^d x \, e^{-ip(x-y)} \langle 0|T\phi^i(x)\phi^k(y)|0\rangle_{conn} \tag{4.1}$$

at two–loop order. According to the formula (3.11), the topology of the graphs is the same as in $O(N)$ theory, except for the term proportional to $\boldsymbol{\phi}^6$. We may therefore again simplify the calculation by evaluating the tree and tadpole diagrams displayed in Fig. 3, with an appropriate choice for the propagators and for the interaction vertex, and to add the sunset diagram Fig. $2\mathrm{d}_{10}$, using the vertices that correspond to $\mathcal{L}_2$. Finally, the term from a_2 generates the butterfly diagram Fig. 6. Collecting these contributions, we find

$$\triangle^{ik}(p^2) = \left\{ \frac{Z}{M_\pi^2 - p^2} + R(p^2) \right\} \delta^{ik} \quad , \tag{4.2}$$

where

$$\begin{aligned} M_\pi^2 &= M^2 + \frac{M^4}{F^2}\left\{2l_3 + \frac{T_M}{2M^2}\right\} + \frac{M^6}{F^4}\dot{T}_M \left\{ Q^M \dot{T}_M - \sum_{i=1}^{3} Q_i^M \, l_i \right\} + \frac{M^6 \, r_M}{F^6} + O(M^8), \\ Z &= 1 - \frac{T_M}{F^2} + \frac{M^4}{F^4}\dot{T}_M \left\{ Q^Z \dot{T}_M - \sum_{i=1}^{3} Q_i^Z \, l_i \right\} + \frac{M^4 \, r_Z}{F^4} + O(M^6) \quad , \end{aligned} \tag{4.3}$$

where [24]

$$\begin{aligned} Q^M &= \frac{1}{96}\left\{204 - 632w + 1263w^2\right\} + O(w^3) \quad , \\ Q_1^M &= \frac{1}{2}\left\{28 - 30w + 31w^2\right\} + O(w^3) \quad , \\ Q_2^M &= 8 - 10w + 11w^2 + O(w^3) \quad , \\ Q_3^M &= 3 - 4w + 4w^2 + O(w^3) \quad , \end{aligned} \tag{4.4}$$

and [24]

$$\begin{aligned} Q^Z &= \frac{1}{96}\left\{96 - 464w + 1185w^2\right\} + O(w^3) \quad , \\ Q_1^Z &= Q_1^M \quad , \; Q_2^Z = Q_2^M \quad , \; Q_3^Z = 2 \, . \end{aligned} \tag{4.5}$$

The function $R(p^2)$ in the propagator is regular at $p^2 = M_\pi^2$. It is not needed in the following, and we no not display its explicit form [24] here. The quantities r_M and r_Z denote the counterterm contributions from the lagrangian $\mathcal{L}_6$. We note that r_M renders the pion mass finite at two–loop order.

4.2 Pion decay constant

We consider the correlators of two pseudoscalar currents [2],

$$\begin{aligned} G^{ik}(p^2) &= i\int d^dx\, e^{-ip(x-y)}\langle 0|T\bar{q}_x i\gamma_5\tau^i q_x \bar{q}_y i\gamma_5\tau^k q_y|0\rangle_{conn} \ , \\ \bar{q} &= (\bar{u},\bar{d}) \end{aligned} \tag{4.6}$$

at two–loop order. Apart from the overall normalization, G^{ik} differs from the two–point function $\triangle^{ik}$ only by terms generated by the low–energy constants l_3 and l_4 (and, of course, by the counterterms from $\mathcal{L}_6$). We find

$$G^{ik}(p^2) = \left\{ \frac{G_\pi^2}{M_\pi^2 - p^2} + R_\pi(p^2) \right\} \delta^{ik} \ , \tag{4.7}$$

where

$$\begin{aligned} G_\pi^2 &= G^2\left[1 + \frac{M^2}{F^2}\left\{2l_4 - 4l_3 - \frac{T_M}{M^2}\right\} + \frac{M^4}{F^4}\dot{T}_M\left\{Q^G\dot{T}_M - \sum_{i=1}^4 Q_i^G l_i\right\}\right. \\ &\quad \left. + \frac{M^4}{F^4}\left\{l_4^2 + 8l_4l_3 + 4l_3^2 + r_G\right\}\right] + O(M^6) \ , \end{aligned} \tag{4.8}$$

with

$$\begin{aligned} G &= 2FB \ , \\ Q^G &= Q^Z \ , \ Q_1^G = Q_1^Z \ , \ Q_2^G = Q_2^Z \ , \\ Q_3^G &= 2(8 - 7w + 7w^2) + O(w^3) \ , \\ Q_4^G &= 1 - w + w^2 + O(w^3) \ . \end{aligned} \tag{4.9}$$

The counterterm contribution from $\mathcal{L}_6$ is denoted by r_G. It renders G_π finite at two–loop order. The regular part R_π is not needed in the following, and we therefore do not display it here.

The relation between the divergence of the axial current and the pseudoscalar density implies

$$F_\pi M_\pi^2 = \hat{m} G_\pi \ . \tag{4.10}$$

The above expressions for the pion mass and for the residue G_π therefore allow us to calculate the pion decay constant to two loops:

$$F_\pi = F\left[1 + \frac{M^2}{F^2}\left\{l_4 - \frac{T_M}{F^2}\right\} + \frac{M^4}{F^4}\left\{r_F + \dot{T}_M\left(Q^F\dot{T}_M - \sum_{i=1}^4 Q_i^F l_i\right)\right\}\right] + O(M^6) \ , \tag{4.11}$$

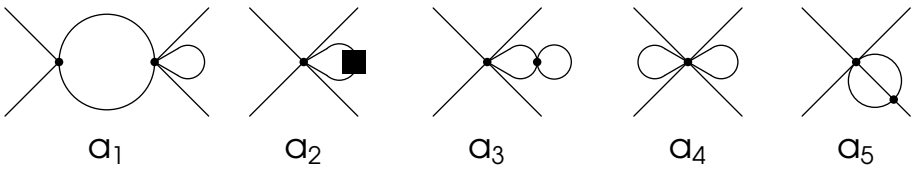

Figure 7: Contributions to elastic $\pi\pi$ scattering in CHPT. The graphs displayed have a different topology than the ones occurring in ϕ^4 theory. The filled box denotes a contribution proportional to the low–energy constant l_3. Graph a_1 is included by use of the formula indicated in Fig. 5, whereas graphs $\mathrm{a}_2 \cdots \mathrm{a}_5$ are not. These must be taken into account separately.

with

$$\begin{aligned} Q^F &= -\frac{1}{192}(240 - 656w + 1125w^2) + O(w^3) \ , \\ Q_1^F &= -\frac{1}{2}Q_1^G \ , \ Q_2^F = -\frac{1}{2}Q_2^G \ , \ Q_3^F = 2 \ , \ Q_4^F = \frac{1}{2}Q_4^G \ . \end{aligned} \tag{4.12}$$

The counterterm contribution from $\mathcal{L}_6$ is denoted by r_F. It renders F_π finite at two–loop order.

4.3 The $\pi\pi$ scattering amplitude

We have discussed in Sect. 2 how one can simplify the calculation of the elastic scattering amplitude in the N–component ϕ^4 theory by using the renormalized one–loop amplitude as a single nonlocal vertex. In case of CHPT, there are a few modifications to be taken into account:

1. As we discussed already in the case of the pion mass and pion decay constant, there are additional diagrams to be taken into account, see the formula (3.11). Some are displayed in Fig. 7. The first of these is taken care of by using the formula illustrated in Fig. 5, whereas the tadpole (Fig. $7\mathrm{a}_2$), the butterfly (Figs. $7\mathrm{a}_3$,a_4) and sunset diagram (Fig. $7\mathrm{a}_5$) have to be added by hand.

2. Since the effective lagrangian in CHPT has derivative interactions, the vertices entering the calculation have a nontrivial off–shell behaviour. This means that the one–loop amplitude entering the above formulae must first be calculated with the appropriate off–shell legs in d dimensions. Since the relevant expression is not available in the literature, we display it in appendix B.

Needless to say that, despite the labour saving organization of the calculation that we just described, it is still rather long and tedious.

In analogy to what we have presented above, we might now display the amplitude in d dimensions. Since the expression is rather long, we prefer to display only the renormalized final expression.

We use the notation

$$\begin{aligned}\langle \pi^d(p_4)\pi^c(p_3)\ \mathrm{out}|\pi^a(p_1)\pi^b(p_2)\ \mathrm{in}\rangle &= \langle \pi^d(p_4)\pi^c(p_3)\ \mathrm{in}|\pi^a(p_1)\pi^b(p_2)\ \mathrm{in}\rangle \\ &+i(2\pi)^4\delta^4(P_f-P_i)\left\{\delta^{ab}\delta^{cd}A(s,t,u)+\mathrm{cycl.}\right\}\ ,\end{aligned}$$

where s,t,u are the usual Mandelstam variables, expressed in units of the physical pion mass squared M_π^2,

$$s \ = \ (p_1+p_2)^2/M_\pi^2\ ,\ t=(p_3-p_1)^2/M_\pi^2\ ,\ u=(p_4-p_1)^2/M_\pi^2\ . \qquad (4.13)$$

Using these dimensionless quantities, the momentum expansion of the amplitude amounts to a Taylor series in

$$x_2 = \frac{M_\pi^2}{F_\pi^2}\ ,$$

where F_π denotes the physical pion decay constant. We find

$$\begin{aligned}A(s,t,u) \ = \ & x_2\,[s-1] \\ &+{x_2}^2\left[b_1+b_2 s+b_3 s^2+b_4(t-u)^2\right] \\ &+{x_2}^2\left[F^{(1)}(s)+G^{(1)}(s,t)+G^{(1)}(s,u)\right] \\ &+{x_2}^3\left[b_5 s^3+b_6 s(t-u)^2\right] \\ &+{x_2}^3\left[F^{(2)}(s)+G^{(2)}(s,t)+G^{(2)}(s,u)\right] \\ &+O({x_2}^4)\ , \end{aligned} \qquad (4.14)$$

with

$$\begin{aligned}F^{(1)}(\,s\,) \ &= \ \frac{1}{2}\,\bar{J}(\,s\,)\,(\,s^2-1\,)\ , \\ G^{(1)}(\,s,t) \ &= \ \frac{1}{6}\,\bar{J}(\,t\,)\,(14\,-\,4\,s\,-\,10\,t\,+\,s\,t\,+\,2\,t^2\,)\ , \\ F^{(2)}(\,s\,) \ &= \ \bar{J}(\,s\,)\left\{\frac{1}{16\pi^2}\left(\frac{503}{108}\,s^3-\frac{929}{54}\,s^2+\frac{887}{27}\,s-\frac{140}{9}\right)\right. \\ &+ \ b_1\,(\,4\,s\,-3)+b_2\,(\,s^2+4\,s\,-4) \\ &+ \ \left.\frac{b_3}{3}\,(\,8\,s^3-21\,s^2+48\,s-32\,)+\frac{b_4}{3}\,(\,16\,s^3-71\,s^2+112\,s-48\,)\right\} \\ &+ \ \frac{1}{18}\,K_1(\,s\,)\left\{20\,s^3-119\,s^2+210\,s-135-\frac{9}{16}\,\pi^2\,(\,s-4\,)\right\} \\ &+ \ \frac{1}{32}\,K_2(\,s\,)\left\{s\,\pi^2-24\right\}+\frac{1}{9}\,K_3(\,s\,)\left\{\,3\,s^2-17\,s+9\,\right\}\ , \\ G^{(2)}(\,s,t\,) \ &= \ \bar{J}(\,t\,)\left\{\frac{1}{16\pi^2}\left[\frac{412}{27}-\frac{s}{54}(t^2+5\,t+159)-t\left(\frac{267}{216}t^2-\frac{727}{108}t+\frac{1571}{108}\right)\right]\right. \\ &+ \ \left.b_1\,(2-t)+\frac{b_2}{3}(t-4)(2\,t+s-5)-\frac{b_3}{6}(t-4)^2(3t+2s-8)\right.\end{aligned}$$

$$
\begin{aligned}
&+ \quad \frac{b_4}{6}\left(2s(3t-4)(t-4)-32t+40t^2-11t^3\right)\Big\} \\
&+ \quad \frac{1}{36}K_1(\,t\,)\left\{\,174+8\,s-10\,t^3+72\,t^2-185\,t-\frac{\pi^2}{16}\,(\,t-4\,)\,(\,3\,s-8\,)\right\} \\
&+ \quad \frac{1}{9}\,K_2(\,t\,)\,\left\{1+4\,s+\frac{\pi^2}{64}\,t\,(\,3\,s-8\,)\,\right\} \\
&+ \quad \frac{1}{9}\,K_3(\,t\,)\left\{1+3st-s+3t^2-9t\right\}+\frac{5}{3}\,K_4(\,t\,)\,\{\,4-2\,s-t\,\}\ . \quad (4.15)
\end{aligned}
$$

The loop functions $\bar{J}$ and K_i are

$$
\begin{pmatrix} \bar{J} \\ K_1 \\ K_2 \\ K_3 \end{pmatrix} = \begin{pmatrix} 0 & 0 & z & -4N \\ 0 & z & 0 & 0 \\ 0 & z^2 & 0 & 8 \\ Nzs^{-1} & 0 & \pi^2(Ns)^{-1} & \pi^2 \end{pmatrix} \begin{pmatrix} h^3 \\ h^2 \\ h \\ -(2N^2)^{-1} \end{pmatrix} \ ,
$$

and

$$
K_4 \ = \ \frac{1}{sz}\left(\frac{1}{2}K_1+\frac{1}{3}K_3+\frac{1}{N}\bar{J}+\frac{(\pi^2-6)s}{12N^2}\right) \ ,
$$

where

$$
h(s)=\frac{1}{N\sqrt{z}}\ln\frac{\sqrt{z}-1}{\sqrt{z}+1} \quad , \qquad z=1-\frac{4}{s}\ ,\ N=16\pi^2\ .
$$

The functions $s^{-1}\bar{J}$ and $s^{-1}K_i$ are analytic in the complex s–plane (cut along the positive real axis for $s \geq 4$), and they vanish as $|s|$ tends to infinity. Their real and imaginary parts are continuous at $s=4$. The coefficients b_i in the polynomial part are given in appendix D.

Finally, we compare our result with the calculation performed in Ref. [9]. There are two basic differences between the two works. First, the present calculation is done in conventional chiral perturbation theory [2], whereas the authors of [9] work in a scenario in which the quark condensate may be small or zero [32] (generalized chiral perturbation theory). The second difference concerns the use of a lagrangian framework in the present approach, whereas S–matrix methods are applied in [9]: Starting from the expression for the amplitude at $O(p^4)$, unitarity allows one to determine the absorptive part at $O(p^6)$. One can then construct an amplitude that has exactly these absorptive parts. Of course, this procedure does not determine the polynomial part at this order. To illustrate, the diagrams of Fig. $7a_{2,3,4,5}$ do not have an absorptive part and can therefore not be determined in this manner. There are additional graphs of this kind. In the amplitude given in [9], these diagrams – and further polynomial contributions from graphs that do have an absorptive part – are lumped into a polynomial

$$
a_1+a_2s+a_3s^2+a_4(t-u)^2+a_5s^3+a_6s(t-u)^2 \qquad (4.16)
$$

with a priori unknown coefficients that depend on the pion mass and on the low–energy constants.

With this procedure, one does not have to work out individual Feynman diagrams, because only the total absorptive part at $O(p^6)$ – fixed through unitarity by the amplitude at $O(p^4)$ – is needed. In addition, the expansion of the pion mass, of the pion decay constant and of the wave function renormalization need not be worked out at $O(p^6)$.

On the other hand, our result (4.14, 4.15) at $O(p^6)$ – obtained by painstakingly evaluating in the manner described above all the Feynman diagrams generated by the effective lagrangian (3.1) – reveals in addition to the findings of [9] the dependence of the six coefficients a_i (4.16) on the pion mass and on the low–energy constants of both $O(p^4)$ and $O(p^6)$, see appendix D. In particular, we find that these coefficients contain mass singularities that are known to be important numerically both at $O(p^4)$ [6, 2] and at $O(p^6)$ [19, 10] (see also Refs. [23, 24, 33]). Furthermore, the knowledge of the mass dependence of the amplitude allows one to evaluate all quantities even at unphysical values of the quark mass, and to confront the result with lattice calculations [34]. This is not possible with the amplitude provided in Ref. [9].

We have checked that the amplitude of [9] (restricted to standard CHPT) and the field theoretic calculation presented here agree as far as the absorptive part of the amplitude and the general structure of the real part is concerned.

5 Numerical analysis

The elastic $\pi\pi$ scattering amplitude is expressed in terms of the external momenta, the physical pion mass, the physical pion decay constant, and the coefficients b_i,

$$A(s,t,u) = f(p_1,\ldots,p_4; M_\pi, F_\pi; b_1,\ldots,b_6)\ .$$

Before one can perform a numerical analysis, one thus needs an estimate of the low–energy couplings b_i. The key relations (D.1) used in [10] for that purpose fix the b_i in terms of

- chiral logarithms $L = \dfrac{1}{16\pi^2}\ln\dfrac{M_\pi^2}{\mu^2}$,
- the low–energy couplings $l_1^r(\mu),\ldots,l_4^r(\mu)$ from $\mathcal{L}_4$,
- the low–energy couplings $r_1^r(\mu),\ldots,r_6^r(\mu)$ generated by $\mathcal{L}_6$.

For a given set of the low–energy constants l_i^r it, therefore, suffices to estimate the new couplings r_i^r at $O(p^6)$. To achieve an order–of–magnitude estimate, we use a method that has been successfully tested at $O(p^4)$ [2, 35]: We work out the contributions from exchanges of heavy states to the scattering amplitude and assume that these effects account for the bulk part in the low–energy couplings at $O(p^6)$. In particular, we include the effect of meson resonance exchange with masses smaller than 1 GeV, i.e., vector and scalar resonances. In addition, we also consider kaon and eta contributions of $O(p^6)$. We describe in the following subsection the relevant resonance couplings and work out the corresponding values for the r_i.

5.1 Resonance saturation

5.1.1 Vector meson exchange

At $O(p^4)$, the contributions of vector meson resonances to the low–energy constants are obtained most naturally with the tensor field representation of spin-1 mesons [2, 36]. The situation is different at $O(p^6)$ where the more common vector field formalism produces directly the relevant counterterm couplings, as observed previously for Compton scattering on pions and for $\gamma\gamma \to \pi\pi$ [37, 23]. We follow the same procedure here and comment later on the difference to the tensor field representation.

The relevant couplings of the vector field $\hat{V}_\mu$, representing the octet of vector mesons (the singlet does not contribute to $\pi\pi$ scattering), to the pseudoscalar mesons are given by [36]

$$\mathcal{L}_V = -\frac{ig_V}{2\sqrt{2}}\left\langle \hat{V}_{\mu\nu}[u^\mu, u^\nu]\right\rangle + f_\chi \left\langle \hat{V}_\mu [u^\mu, \chi_-]\right\rangle \tag{5.1}$$

$$\hat{V}_{\mu\nu} = \nabla_\mu \hat{V}_\nu - \nabla_\nu \hat{V}_\mu$$

with real dimensionless coupling constants g_V, f_χ. We switch to chiral $SU(3)$ here (and also in the next subsection for the discussion of scalar exchange) to determine both couplings g_V, f_χ from vector meson decays. From the Lagrangian (5.1) one finds that the combination

$$g_V + 2\sqrt{2} f_\chi \frac{M_1^2 + M_2^2}{M_V^2}$$

determines the amplitude for the decay of a vector meson into two pseudoscalars. From the experimental widths for $\rho \to \pi\pi$ and $K^* \to K\pi$ one obtains $g_V f_\chi < 0$ with

$$g_V = 0.09\ , \qquad f_\chi = -0.03\ , \tag{5.2}$$

if we define g_V to be positive. V exchange on the basis of (5.1) gives rise to three types of contributions proportional to g_V^2, $g_V f_\chi$ and f_χ^2, respectively. With

$$\begin{aligned} a_V &= \frac{g_V^2 F_\pi^2}{M_V^2} = 1.2 \cdot 10^{-4} \\ b_V &= \frac{4\sqrt{2} g_V f_\chi F_\pi^2}{M_V^2} = -2.2 \cdot 10^{-4} \\ c_V &= \frac{32 f_\chi^2 F_\pi^2}{M_V^2} = 4.2 \cdot 10^{-4}\ , \end{aligned}$$

using $M_V = M_\rho$ for the numerical values, we obtain the following V exchange contributions to the low–energy constants r_i:

$$\begin{aligned} r_1^V &= -16a_V - 16b_V - 4c_V \\ r_2^V &= 20a_V + 16b_V + 3c_V \\ r_3^V &= -7a_V - 3b_V \end{aligned} \tag{5.3}$$

$$
\begin{aligned}
r_4^V &= a_V + b_V \\
r_5^V &= \frac{3}{4} a_V \\
r_6^V &= \frac{1}{4} a_V \ .
\end{aligned}
$$

In the tensor field representation, there is a single coupling (relevant for $\pi\pi$ scattering) between vector mesons and pseudoscalars at lowest order [2, 35]. Up to normalization, the corresponding coupling constant is given by g_V . For instance, expanding the ρ exchange amplitude of Ref. [2] to $O(p^6)$ is equivalent to (5.3) with $b_V = c_V = 0$. Higher–order couplings can only contribute at $O(p^6)$ through interference with the g_V amplitude. Thus, the contributions involving f_χ^2 that appear naturally in the vector field formalism would have to be added by hand in the tensor field representation as explicit local counterterms.

5.1.2 Scalar meson exchange

To estimate the effect of scalar resonances for the r_i, we take the lowest–order lagrangian of Ref. [35] for octet and singlet scalar fields S, S_1,

$$
\mathcal{L}_S = c_d \left\langle S u^\mu u_\mu \right\rangle + c_m \left\langle S \chi_+ \right\rangle + \widetilde{c_d} S_1 \left\langle u^\mu u_\mu \right\rangle + \widetilde{c_m} S_1 \left\langle \chi_+ \right\rangle \ , \tag{5.4}
$$

and expand the resonance exchange amplitudes up to $O(p^6)$. The resulting scalar contributions to the r_i are:

$$
\begin{aligned}
r_1^S &= 0 \\
r_2^S &= \frac{8F_\pi^2}{3M_S^4}(c_m - c_d)^2 + \frac{16F_\pi^2}{M_{S_1}^4}(\widetilde{c_m} - \widetilde{c_d})^2 \\
r_3^S &= \frac{8F_\pi^2}{3M_S^4} c_d (c_m - c_d) + \frac{16F_\pi^2}{M_{S_1}^4} \widetilde{c_d}(\widetilde{c_m} - \widetilde{c_d}) \\
r_4^S &= 0 \\
r_5^S &= \frac{2F_\pi^2}{3M_S^4} c_d^2 + \frac{4F_\pi^2}{M_{S_1}^4} \widetilde{c_d}^2 \\
r_6^S &= 0 \ .
\end{aligned} \tag{5.5}
$$

Note that the physical pion mass and the physical pion decay constant receive contributions from scalar exchange as well.

For the numerical evaluation we use the same values for masses and coupling constants as in Ref. [35]:

$$
\begin{aligned}
M_S = M_{S_1} &= 983 \text{ MeV} \\
c_m = 42 \text{ MeV} \ , \qquad & c_d = 32 \text{ MeV} \\
\widetilde{c_m} = c_m/\sqrt{3} \ , \qquad & \widetilde{c_d} = c_d/\sqrt{3} \ .
\end{aligned}
$$

5.1.3 Kaon and eta contributions

In the framework of chiral $SU(3)$, K and η mesons contribute at $O(p^4)$ to $\pi\pi$ scattering via loop diagrams. Restricting the scattering amplitude of $O(p^4)$ evaluated in chiral $SU(3)$ [9] to $SU(2) \times SU(2)$ by an expansion in inverse powers of the strange quark mass, one arrives at the following contributions to the r_i due to K and η mesons:

$$\begin{aligned} r_1^K &= \frac{31F_\pi^2}{5760\pi^2 M_K^2} \\ r_2^K &= -\frac{11F_\pi^2}{2304\pi^2 M_K^2} \\ r_3^K &= -\frac{29F_\pi^2}{7680\pi^2 M_K^2} \\ r_4^K &= -\frac{F_\pi^2}{2560\pi^2 M_K^2} \\ r_5^K &= \frac{23F_\pi^2}{15360\pi^2 M_K^2} \\ r_6^K &= \frac{F_\pi^2}{15360\pi^2 M_K^2} \ . \end{aligned} \tag{5.6}$$

5.1.4 Numerical values of the r_i

Putting the various contributions of the previous subsections together, we obtain the following numerical estimates for what we shall call the resonance contributions to the low–energy constants of $O(p^6)$:

$$\begin{aligned} r_1^R &= -0.6 \cdot 10^{-4} \\ r_2^R &= 1.3 \cdot 10^{-4} \\ r_3^R &= -1.7 \cdot 10^{-4} \\ r_4^R &= -1.0 \cdot 10^{-4} \\ r_5^R &= 1.1 \cdot 10^{-4} \\ r_6^R &= 0.3 \cdot 10^{-4} \ . \end{aligned} \tag{5.7}$$

These values are the ones used in Ref. [10]. They indicate an $O(p^6)$ version of vector meson dominance: Despite some strong cancellations (especially for r_1^V, r_2^V), all six constants r_i^R are dominated by the exchange of vector mesons.[5]

Of course, the constants b_i become scale dependent if we now replace the $r_i^r(\mu)$ by the above r_i^R. At $O(p^4)$, the empirically observed resonance saturation of low–energy constants amounts to the statement [35] that the resonance contributions describe the phenomenologically determined coupling constants quite well for a scale μ between 500 MeV and 1 GeV. Pending a more refined analysis along the lines

[5] Other estimates of the low–energy constants of $O(p^6)$ can be found in Refs. [38].

discussed below, we assume for the time being that the same approximation is meaningful also at $O(p^6)$. Of course, only observables that are relatively insensitive to scale changes in the range mentioned can be estimated in a reasonable manner in this way.

5.2 The constants b_i

Together with the couplings l_i^r at $O(p^4)$, the estimates (5.7) allow one to work out the constants $b_1, \ldots, b_6$. We used in Ref. [10] values for the l_i^r that were determined mainly from an $O(p^4)$ analysis [2], with additional input from a dispersive estimate of higher–order effects in K_{l4} decays [21]. As emphasized in our previous paper, all those determinations were faced with the problem that the l_i are mass independent, whereas the physical quantities, from which the l_i^r were determined, include quark mass effects. We will illustrate below the relevance of those quark mass effects by example.

With the scale–independent couplings $\bar{l}_i$ (cf. App. D) found in [2, 21],

$$\begin{aligned} \bar{l}_1 &= -1.7 \ , \quad \bar{l}_2 = 6.1 \ , \\ \bar{l}_3 &= 2.9 \ , \quad \bar{l}_4 = 4.3 \ , \end{aligned} \tag{5.8}$$

and with the constants r_i^R in (5.7), one arrives[6] at the b_i displayed in table 1. There, we have split the contributions to the b_i into one–loop and two–loop effects. Furthermore, we indicate separately the contributions from the r_i^R. The values shown correspond to the scale $\mu = 1$ GeV ($\mu = 500$ MeV in brackets). (We display the values to two digits for ease of reproduction of the numbers.) Below we refer to the b_i in this table as set I. The following remarks are in order.

Table 1: The constants b_i (set I). We use Eqs. (5.7,5.8) as input to evaluate b_i from Eq. (D.1). The numbers correspond to $\mu = 1$ GeV, in brackets we display the corresponding values at $\mu = 500$ MeV.

	1-loop	2-loops, r_i=0	from r_i^R	total
$10^2 b_1$	-7.34	-1.76 (-1.82)	-0.01	-9.11 (-9.17)
$10^2 b_2$	6.74	2.07 (2.12)	0.03	8.84 (8.89)
$10^3 b_3$	-0.84	-3.05 (-3.43)	-0.38	-4.27 (-4.65)
$10^3 b_4$	5.56	1.72 (1.71)	-0.22	7.05 (7.04)
$10^4 b_5$		1.22 (1.24)	1.10	2.32 (2.34)
$10^4 b_6$		1.19 (0.77)	0.30	1.49 (1.07)

[6] As in Ref. [10], we use $F_\pi = 93.2$ MeV, $M_\pi = 139.57$ MeV.

i) The change induced by $\mu = 1$ GeV $\to \mu = 500$ MeV is of the same order or bigger than the contributions from r_i^R (see also table 3), with the possible exception of b_4.

ii) Besides the scale dependence, there is yet another source of uncertainty that has to do with using the EOM in the lagrangian of $O(p^4)$. As discussed in Sects. 2 (for ϕ^4) and 3 (for CHPT), this ambiguity can always be resolved by a redefinition of the coupling constants of $O(p^6)$ – physical observables are of course unaffected. Although this is a completely general result for the generating functional to $O(p^6)$ [27], we nevertheless face a practical problem here because our estimates of the r_i^r via resonance exchange are not only scale independent but they also make no reference to the form of the lagrangian of $O(p^4)$. We have checked that using the $O(p^4)$ lagrangians of either Ref. [2] or of Ref. [39] induces a change in $b_{1,2,3,4}$ by an amount that is smaller than the change due to a different choice of scale. The constants $b_{5,6}$ are unaffected by this procedure.

iii) The main uncertainties in the b_i stem from the couplings of $O(p^4)$, as we now illustrate. In table 2, we have displayed the contributions from $\bar{l}_i$ to b_i at one–loop order. They are at least an order of magnitude bigger than the ones from the r_i^R – therefore, uncertainties in the latter are swamped by uncertainties in the $\bar{l}_i$. One of these are quark mass effects, mentioned above. To illustrate these, we repeat the analysis of Ref. [2] to fix $\bar{l}_1$, $\bar{l}_2$ from the D–wave scattering lengths a_2^0, a_2^2, but now to $O(p^6)$. Keeping $\bar{l}_3$, $\bar{l}_4$ fixed, the experimental values [40] given in table 4 lead to

$$\begin{aligned} \bar{l}_1 &= -1.5 \\ \bar{l}_2 &= 4.5 \end{aligned} \tag{5.9}$$

if $\bar{l}_3, \bar{l}_4$ from (5.8) are used as input. The b_i that result from this exercise are displayed in table 3 and referred to as set II in the following. Since $b_{1,2}$ do not depend on $\bar{l}_2$, they remain largely unaffected, whereas the change in $b_{3,\ldots,6}$ is seen to be substantial. The values (5.9) should be compared with the values obtained at $O(p^4)$, $\bar{l}_1 = -2.3$ and $\bar{l}_2 = 6.0$, from the same input [2]. Values similar to (5.9) were found in [20] comparing a Roy equation fit to our p^6 amplitude [10].

iv) Similar effects are expected from changes in $\bar{l}_4$ that does contribute substantially to $b_{1,2}$. As we already mentioned in our previous work [10], a more detailed analysis is therefore needed to obtain reliable values for the $\bar{l}_i$, consistent with an analysis at $O(p^6)$, and, at the same time, values for the b_i with error bars attached. Such an analysis is under way [41].

v) This brings us to the work of Ref. [18] who find from dispersion sum rules the

Table 2: Contributions from the individual $\bar{l}_i$ in Eq. (5.8) to the constants b_i in the one–loop approximation. Note that $b_{5,6}$ start at two–loop order.

1-loop	$\bar{l}_1$	$\bar{l}_2$	$\bar{l}_3$	$\bar{l}_4$	analytic	total
$10^2 b_1$	-1.44	0	-0.92	-5.44	0.46	-7.34
$10^2 b_2$	1.44	0	0	5.44	-0.14	6.74
$10^3 b_3$	-3.59	6.44	0	0	-3.69	-0.84
$10^3 b_4$	0	6.44	0	0	-0.88	5.56

Table 3: The constants b_i (set II). We use Eqs. (5.7,5.9) as input to evaluate b_i from Eq. (D.1). The numbers correspond to $\mu = 1$ GeV, in brackets we display the corresponding values at $\mu = 500$ MeV.

	1-loop	2-loops, r_i=0	from r_i^R	total
$10^2 b_1$	-7.17	-1.44 (-1.62)	-0.01	-8.63 (-8.80)
$10^2 b_2$	6.57	1.41 (1.71)	0.03	8.01 (8.31)
$10^3 b_3$	-2.11	-0.14 (-1.85)	-0.38	-2.63 (-4.34)
$10^3 b_4$	3.87	1.17 (1.20)	-0.22	4.82 (4.85)
$10^4 b_5$		-1.47 (-0.22)	1.10	-0.37 (0.88)
$10^4 b_6$		0.53 (0.42)	0.30	0.83 (0.72)

values

$$\left.\begin{aligned} b_3 &= (-3.7 \pm 2.4) \cdot 10^{-3} \\ b_4 &= (4.8 \pm 0.3) \cdot 10^{-3} \\ b_5 &= (1.4 \pm 0.6) \cdot 10^{-4} \\ b_6 &= (1.0 \pm 0.1) \cdot 10^{-4} \end{aligned}\right\} \tag{5.10}$$

Within the error bars quoted, these values are consistent with our set II. The theoretical framework used in [18] does not allow these authors to determine $b_{1,2}$ – rather, these quantities can in principle be determined from precise data on elastic $\pi\pi$ scattering, allowing then a determination of the size of the quark condensate in the chiral limit.

vi) Recently, Wanders has also extracted the $b_{3,4,5,6}$ using crossing–symmetric sum rules [11]. Taking the $O(p^4)$ expressions for b_1, b_2 as input, he finds that at

$O(p^6)$ three of the b_i are only weakly sensitive to the choice of the energy separating high– and low–energy components in the sum rules. The resulting values (for the interpretation of the errors we refer to [11])

$$\left.\begin{aligned} b_3 &= (-2.55 \pm 0.20) \cdot 10^{-3} \\ b_4 &= (4.55 \pm 0.15) \cdot 10^{-3} \\ b_6 &= (0.92 \pm 0.03) \cdot 10^{-4} \end{aligned}\right\} \tag{5.11}$$

are consistent with our set II and with the values (5.10) of Knecht et al. [18].

5.3 Threshold parameters and phase shifts

To compare the theoretical amplitudes with data on $\pi\pi$ scattering, one expands the combinations with definite isospin in the s-channel

$$\begin{aligned} T^0(s,t) &= 3A(s,t,u) + A(t,u,s) + A(u,s,t) \\ T^1(s,t) &= A(t,u,s) - A(u,s,t) \\ T^2(s,t) &= A(t,u,s) + A(u,s,t) \end{aligned} \tag{5.12}$$

into partial waves,

$$T^I(s,t) = 32\pi \sum_{l=0}^{\infty} (2l+1) P_l(\cos\theta) t_l^I(s) \; . \tag{5.13}$$

Unitarity implies that in the elastic region[7] $4 \leq s \leq 16$ the partial wave amplitudes t_l^I are described by real phase shifts δ_l^I,

$$t_l^I(s) = \left(\frac{s}{s-4}\right)^{1/2} \frac{1}{2i} \{ e^{2i\delta_l^I(s)} - 1 \} \; . \tag{5.14}$$

The behaviour of the partial waves near threshold is of the form

$$\mathrm{Re}\; t_l^I(s) = q^{2l} \{ a_l^I + q^2 b_l^I + O(q^4) \} \; , \tag{5.15}$$

with q the center–of–mass three–momentum of the pions, i.e. $s = 4(1 + q^2/M_\pi^2)$. The threshold parameters a_l^I, b_l^I are referred to as scattering lengths and slope parameters, respectively.

In table 4, we compare the threshold parameters of the low partial waves with experimental results. We emphasize once more that we do not consider the values for either set I or set II as the definitive results of $O(p^6)$. To arrive at such results, a more detailed analysis based on the Roy–equation approach is under way [41]. With this caveat in mind, we notice that the $\bar{l}_1$, $\bar{l}_2$ from the D–wave scattering lengths (set II) tend to improve the agreement with experiment with the possible exception of the S–wave scattering lengths a_0^0, a_0^2. We comment on the experimental determinations of scattering lengths below. We also note that the ambiguity in scale or in the choice of the lagrangian of $O(p^4)$ affects a_0^0 in the third digit only.

[7] We recall our normalization of the Mandelstam variables in (4.13).

Table 4: Threshold parameters in units of M_{π^+}. The values of $O(p^4)$ and $O(p^6)$ (set I) correspond to $\bar{l}_1 = -1.7$, $\bar{l}_2 = 6.1$, $\bar{l}_3 = 2.9$, $\bar{l}_4 = 4.3$. For $O(p^6)$ (set II), $\bar{l}_1 = -1.5$, $\bar{l}_2 = 4.5$ were extracted from the D–wave scattering lengths ($\bar{l}_3$, $\bar{l}_4$ unchanged). The fourth column shows the values obtained taking only the contributions from the k_i [19] defined in App. D. We set $\mu = 1$ GeV and take the $r_i^r(1\text{ GeV})$ from (5.7). The experimental values are from Ref. [40].

	$O(p^2)$	$O(p^4)$	$O(p^6)$ set I		$O(p^6)$	experiment
			k_i	all	set II	
a_0^0	0.16	0.20	0.213	0.217	0.206	0.26 ± 0.05
b_0^0	0.18	0.25	0.279	0.275	0.249	0.25 ± 0.03
$-10\ a_0^2$	0.45	0.42	0.407	0.413	0.443	0.28 ± 0.12
$-10\ b_0^2$	0.91	0.73	0.69	0.72	0.80	0.82 ± 0.08
$10\ a_1^1$	0.30	0.37	0.40	0.40	0.38	0.38 ± 0.02
$10^2 b_1^1$	0	0.48	0.78	0.79	0.54	
$10^2 a_2^0$	0	0.18	0.30	0.27	input	0.17 ± 0.03
$10^3 a_2^2$	0	0.21	0.34	0.23	input	0.13 ± 0.30

In Figs. 8, 9 we plot the phase shift difference $\delta_0^0 - \delta_1^1$ and the $I = 2$ S–wave phase shift δ_0^2 as functions of the center–of–mass energy and compare with the available low–energy data. The phase shifts correspond to the amplitudes of $O(p^2)$, $O(p^4)$ and $O(p^6)$ (for both sets I and II), respectively. The two–loop phase shifts describe the K_{e4} data quite well for both sets of $\bar{l}_i$, with a small preference for set I. The $I = 2$ S–wave, on the other hand, seems to prefer set II.

There is an interesting lesson we can draw from our amplitude concerning the extraction of threshold parameters from phase shift data. Looking at Fig. 8, we observe that the p^6 amplitude (set I) describes the data almost perfectly. On the other hand, the value for the scattering length a_0^0 in table 4 is 0.217 for set I, quite a bit smaller than the 0.26 from Ref. [40] and even smaller than the 0.28 from Ref. [42].

To put these differences into perspective, we consider the effective range approximation for S–wave scattering [44],

$$q\ \cot \delta_0^I = \frac{M_\pi}{a_0^I} + \frac{1}{2} r_0^I q^2\ , \tag{5.16}$$

with r_0^I the effective range. In terms of the threshold parameters defined in (5.15),

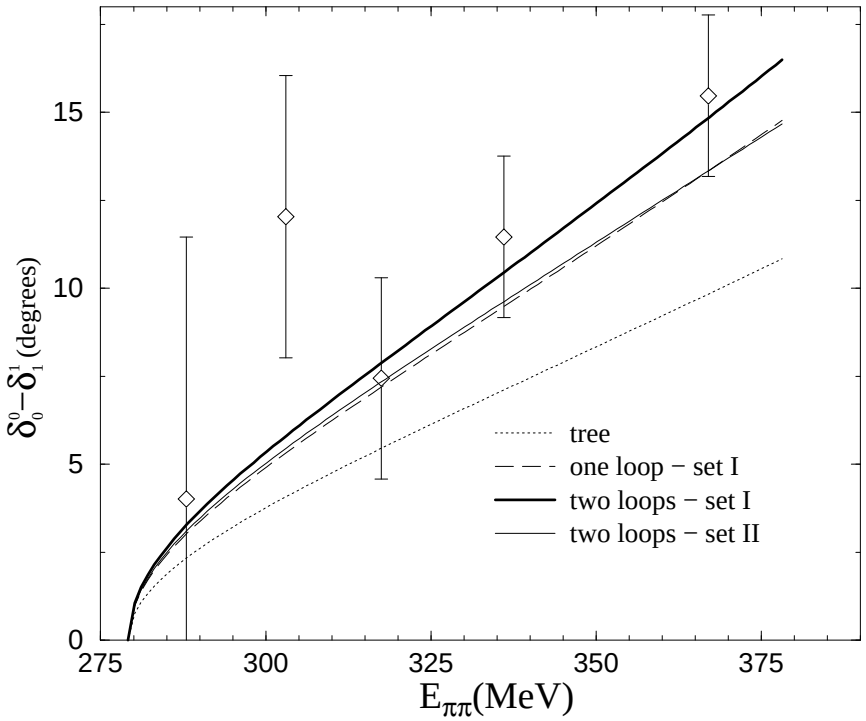

Figure 8: Phase shift difference $\delta_0^0 - \delta_1^1$ at $O(p^2)$, $O(p^4)$ and $O(p^6)$ (set I and II). The data points are from Ref. [42].

the effective range is given by

$$r_0^I = \frac{1}{M_\pi a_0^I} - \frac{2M_\pi b_0^I}{(a_0^I)^2} - \frac{2a_0^I}{M_\pi}\,. \tag{5.17}$$

A similar formula can be used for δ_1^I when we replace (a_0^I, b_0^I) by $(q^2 a_1^I, q^2 b_1^I)$.

In Ref. [42], the following approximation was used to extract the scattering length a_0^0 from the measured phase shifts:

$$\sin 2(\delta_0^0 - \delta_1^1) = 2\sqrt{1-\frac{4}{s}}\,(a_0^0 + q^2 b)\ . \tag{5.18}$$

In addition, a relation between a_0^0 and b attributed to Basdevant et al. [45] was employed for a one–parameter fit to the data.

In Fig. 10, we compare the phase shift difference δ_0^0 - δ_1^1 from the full two–loop calculation (set I) with the effective range formula (5.16) and with the approximation (5.18) used by Rosselet et al. [42]. For the effective range approximation, we have used the threshold parameters corresponding to the CHPT amplitude (set I in table 4). In the curve based on (5.18) we have also used $a_0^0 = 0.217$ and the above mentioned relation [45] between a_0^0 and b.

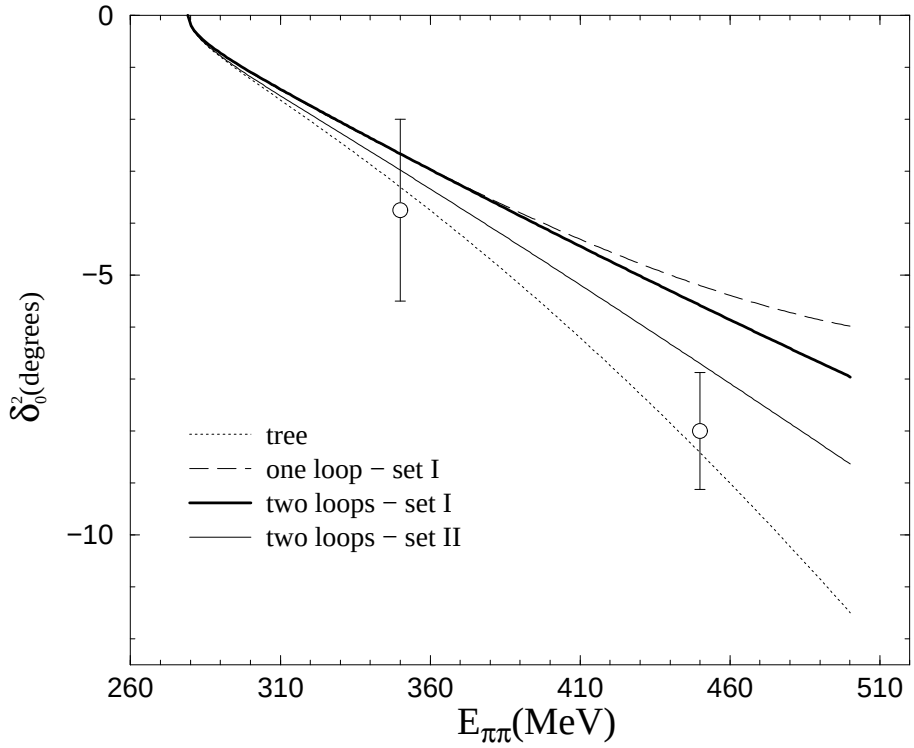

Figure 9: Phase shift δ_0^2 at $O(p^2)$, $O(p^4)$ and $O(p^6)$ (set I and II). The data points are from Ref. [43].

The obvious conclusion is that both the effective range approximation and the approximation used in Ref. [42] deviate from CHPT to $O(p^6)$ already at comparatively low energies. Fig. 10 also shows why the scattering length obtained in Ref. [42] is bigger than the CHPT value. It is hardly necessary to emphasize that the phase shift from CHPT is superior to both approximations on all accounts.

6 Conclusions

In this paper we have presented the calculation of elastic pion–pion scattering to sixth order in the low–energy expansion of QCD. The main part has been devoted to explaining the technical aspects of the results given in [10].

We first developed the loop expansion and the renormalization procedure for the generating functional of Green functions at the one– and two–loop level in the N–component ϕ^4 theory We concentrated on issues that are relevant for the corresponding CHPT calculation. In particular, we have discussed the dependence on the renormalization scheme and the impact of the EOM. Using the EOM, the counterterms in ϕ^4 theory can be written in different ways. We demonstrated explicitly that different choices are equivalent in the sense that the differences can always be

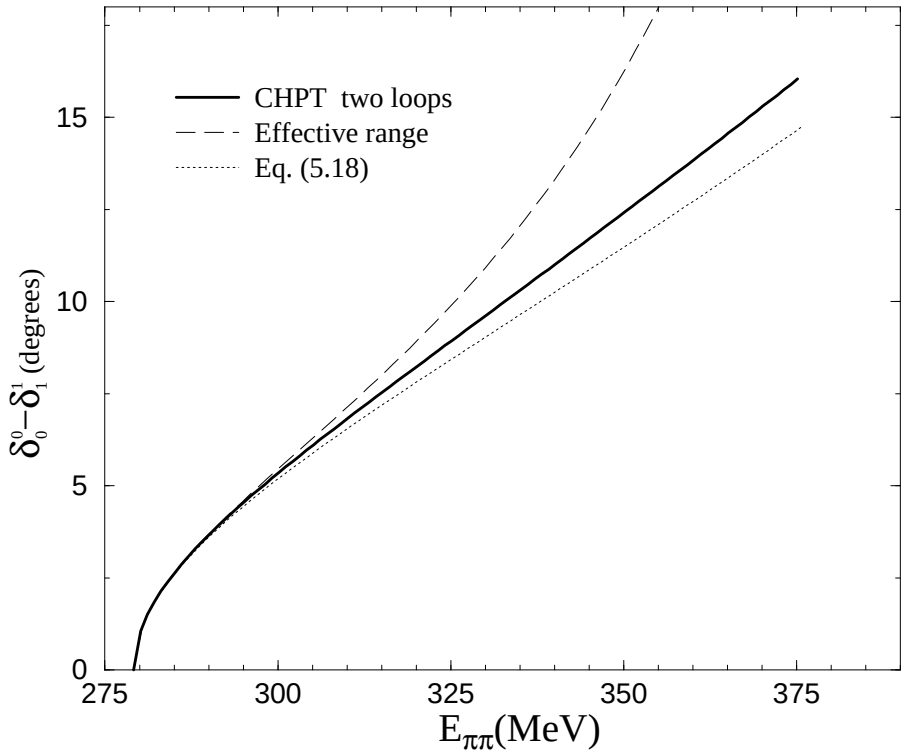

Figure 10: Comparison of the full two–loop phase shift difference $\delta_0^0 - \delta_1^1$ with the effective range formula (5.16) and with Eq. (5.18).

absorbed into the higher–order parameters. We discussed a method for calculating two–loop diagrams by treating the renormalized one–loop amplitude as a nonlocal vertex. This approach turns out to be especially useful for the more involved CHPT calculation.

For the case of CHPT, we then performed the corresponding calculations for the pion mass, the pion decay constant and the $\pi\pi$ scattering amplitude. The renormalization of these quantities to $O(p^6)$ was discussed in detail for both minimal subtraction and for the modified minimal subtraction scheme that we actually used. In analogy to ϕ^4 theory, the role of the EOM in relating different forms of the chiral lagrangian was discussed. We also commented on the Laurent expansion in $d-4$ of the coupling constants of $O(p^4)$.

We determined the complete dependence of M_π, F_π and the scattering amplitude on the quark masses. As in previous full two–loop calculations [23, 24, 33], this dependence is both of theoretical interest and of numerical relevance. The analytical expressions for the scattering amplitude and for the threshold parameters were given.

For the numerical analysis of $\pi\pi$ scattering, we derived estimates of the low–energy constants of $O(p^6)$ on the basis of meson resonance exchange including kaon and eta contributions. These estimates turn out to be dominated by vector meson contributions. Although there are considerable uncertainties in this simple version

of resonance saturation, the overall size of the constants of $O(p^6)$ is such that many quantities are relatively immune to those uncertainties. This is especially the case for the S–waves. However, for the higher partial waves and for a systematic error analysis in general a more sophisticated approach is needed. Such an analysis based on Roy equations is under way [41]. A similar approach has already been used in the dispersive treatment of the scattering amplitude to two–loop order [9, 18].

The major uncertainties for a numerical analysis reside in the low–energy constants of $O(p^4)$. To illustrate this uncertainty, we have presented results both for the standard set of those constants [2, 21] and for a second set where $\bar{l}_1$, $\bar{l}_2$ are determined from the D–wave threshold parameters to $O(p^6)$ as given in this paper. In this case, even the S–waves are sensitive to which set of constants is used. This makes it all the more necessary to perform an analysis where all the constants are determined on the basis of $O(p^6)$ quantities that include, in particular, quark mass effects.

We have also presented numerical results for the phase shifts including the combination that can be measured directly in K_{e4} decays. For this particular example, we demonstrated that approximations like the effective range expansion may deviate from the CHPT predictions already at relatively low energies. We have emphasized the problems of extracting threshold parameters on the basis of such approximations from phase shift data.

The results obtained here for the $\pi\pi$ scattering amplitude to $O(p^6)$ will be used for a systematic analysis [41] of the available experimental data. In addition, they will be the basis for significant tests of QCD at low energies together with forthcoming measurements of $\pi\pi$ scattering near threshold in K_{e4} decays and in pionium decay [46].

Acknowledgements

We would like to thank M. Knecht, H. Leutwyler and J. Stern for useful discussions. This work is supported in part by FWF (Austria), Project No. P09505–MAT, by the Magnus Ehrnrooth Foundation (Finland), by the Swedish Science Research Council (NFR), by the Swiss National Science Foundation, by the Bundesamt für Bildung und Wissenschaft (contract No. 930341), and by HCM, contract No. CHRX–CT920026 (EURODAΦNE).

A Fish and sunset diagrams

A.1 Notation

We use the notation

$$\langle\ldots\rangle = \int \frac{d^dl_1}{i(2\pi)^d}(\ldots) \ , \ \langle\langle\ldots\rangle\rangle = \int \frac{d^dl_1}{i(2\pi)^d}\int \frac{d^dl_2}{i(2\pi)^d}(\ldots) \ ,$$

together with

$$w = \frac{d}{2} - 2 \ .$$

Furthermore, as only one mass parameter occurs in this appendix, we put everywhere $M^2 = 1$. It is straightforward to supplement the quantities below with the relevant mass factors.

The loop function $J(s)$ in d dimensions is

$$\begin{aligned} J(s) &= \left\langle \frac{1}{(1-l_1^2)(1-(l_1-p)^2)} \right\rangle \\ &= \frac{1}{(4\pi)^{2+w}} \Gamma(-w) \int_0^1 dx \, (1 - sx(1-x))^w \;\; ; \;\; p^2 = s \; . \end{aligned} \tag{A.1}$$

For J one has the dispersive representation

$$J(s) = \int_4^\infty \frac{[dx]}{x-s} \;\; ; \;\; -1.5 < w < 0 \;\; , \tag{A.2}$$

where the measure is

$$[dx] = \frac{\Gamma(3/2)}{(4\pi)^{2+w}\Gamma(3/2+w)} \left(\frac{x}{4}\right)^w (1-\frac{x}{4})^{\frac{1}{2}+w} \, dx \; . \tag{A.3}$$

It is often convenient to split off the divergent part through

$$\begin{aligned} J(s) &= J(0) + \bar{J}(s) \;\; , \\ J(0) &= \frac{1}{(4\pi)^{2+w}} \Gamma(-w) \;\; , \\ \bar{J}(s) &= s \int_4^\infty \frac{[dx]}{x(x-s)} \\ &\stackrel{d\to 4}{=} \frac{1}{16\pi^2} \left[\sigma \ln \frac{\sigma - 1}{\sigma + 1} + 2 \right] \;\; ; \;\; \sigma = (1 - 4/s)^{\frac{1}{2}} \; . \end{aligned} \tag{A.4}$$

The constant $J(0)$ is related to $\dot{T}_M$, used in the text, via $\dot{T}_M = -J(0)$ taking into account that $M = 1$ in this appendix.

A.2 The fish diagram

The scalar integral for the fish diagram has the form

$$V(s) = \left\langle \left\langle \prod_{i=1}^4 \frac{1}{D_i} \right\rangle \right\rangle$$

with

$$\begin{aligned} D_1 &= 1 - l_1^2 \;\; , \; D_2 = 1 - (Q - l_1)^2 \;\; , \\ D_3 &= 1 - l_2^2 \;\; , \; D_4 = 1 - (l_2 + l_1 - p_1)^2 \;\; , \\ Q &= p_1 + p_2 \;\; , \; p_1^2 = p_2^2 = 1 \;\; , \; Q^2 = s \; . \end{aligned}$$

We evaluate this integral in two steps: First, we identify that part of the function $V(s)$ that stays finite as $d \to 4$ by subtracting the divergent subintegral and by removing the remaining overall divergence. In the second step, we determine the finite part by evaluating its absorptive part along the cut in the variable s and by then constructing an analytic function that has the same absorptive part and the same behaviour at $s \to 0, -\infty$.

Subtractions

Integration over l_2 generates the loop function $J(\bar{t}), \bar{t} = (p_1 - l_1)^2$. We subtract the divergence in this subdiagram by using the decomposition (A.4) and obtain

$$\begin{aligned} V(s) &= J(s)J(0) + V_1(s) \ , \\ V_1(s) &= \int_4^\infty \frac{[dx]}{x} \left\langle \frac{\bar{t}}{D_1 D_2 (x - \bar{t})} \right\rangle . \end{aligned} \tag{A.5}$$

V_1 is still divergent at $d = 4$. Using the Feynman parametrization

$$\frac{1}{D_1 D_2 (x - \bar{t})} = \int_0^1 \frac{2 x_2 dx_1 dx_2}{\left[(x_1 D_1 + (1 - x_1) D_2)\, x_2 + (x - \bar{t})\,(1 - x_2) \right]^3} \ ,$$

integrating first over l_1 and then by parts in x_1 shows that V_1 can be made finite by subtracting its value at $s = 0$,

$$V_1(s) = V_1(0) + \overline{V}_1(s) \ \ ; \ \ \lim_{s \to -\infty} \frac{\overline{V}_1}{s} = 0 \ .$$

$V_1(0)$ can be evaluated by methods similar to the ones used below for the sunset integral.

The finite part $\overline{V}_1(s)$

To evaluate the absorptive part of $\overline{V}_1(s)$, we invoke unitarity [47]:

$$\begin{aligned} \mathrm{Im} V(s) &= J(0) \mathrm{Im} J(s) + \mathrm{Im} \overline{V}_1(s) \\ &= \frac{(2\pi)^{2w+4}}{2} \int d\mu(l) d\mu(l') \delta^{(d)}(Q - l - l') J(\bar{t}) \ , \end{aligned}$$

where $d\mu$ is the Lorentz invariant measure in d dimensions,

$$d\mu(l) = \frac{d^{2w+3} l}{2 (2\pi)^{2w+3} l^0} \ , \ l^0 = \sqrt{1 + \vec{l}^2} \ , \ . \tag{A.6}$$

We write again $J(\bar{t}) = J(0) + \bar{J}(\bar{t})$ and use

$$\frac{(2\pi)^{2w+4}}{2} \int d\mu(l) d\mu(l') \delta^{(d)}(Q - l - l') \ = \ \frac{\pi \Gamma(3/2)}{(4\pi)^{2+w} \Gamma(3/2 + w)} \left(\frac{s}{4} \right)^w \left(1 - \frac{s}{4} \right)^{\frac{1}{2} + w} \ .$$

This expression agrees with the absorptive part of $J(s)$ in d dimensions, see Eqs. (A.2, A.3). Therefore, at $d = 4$, one has

$$\mathrm{Im}\overline{V}_1(s) = \frac{(2\pi)^4}{2}\int d\mu(l)d\mu(l')\delta^{(4)}(Q-l-l')\bar{J}(\bar{t}) \ , \tag{A.7}$$

where the measure in (A.7) is now the ordinary four–dimensional one, obtained from (A.6) by putting $w = 0$. For $\bar{J}$ we insert its explicit expression (A.4) at $d = 4$. It is convenient to work out the phase space integral (A.7) in the center–of–mass frame where

$$Q^\mu = (\sqrt{s},\vec{0}) \ , \ p_1^\mu = (\sqrt{s}/2,0,0,p) \ , \ p = \sqrt{s/4-1} \ .$$

After integration over l', one is left with an integral over the three–momentum $\vec{l}$. Using the remaining one–dimensional delta function, all integrals except the one over the angle $\theta(\vec{l},\vec{p}_1)$ can be done easily. The integral left over is proportional to

$$\int_{-1}^{1} dz \left[\sigma_1 \ln\frac{\sigma_1-1}{\sigma_1+1}+2\right] \ , \ \sigma_1 = \sqrt{1+\frac{2}{p(1-z)}} \ .$$

After the change of variables $(\sigma_1-1)/(\sigma_1+1) = v$, we find

$$\mathrm{Im}\,\overline{V}_1(s) = \frac{1}{4(4\pi)^3}\left[3\sigma + \ln\frac{1-\sigma}{1+\sigma} - \frac{1}{s\sigma}\ln^2\frac{1-\sigma}{1+\sigma}\right] \ , \ \ \sigma = (1-4/s)^{\frac{1}{2}} \ . \tag{A.8}$$

It remains to construct a function with the proper cut structure and the correct behaviour at $s \to 0, \infty$. We find

$$\overline{V}_1(s) = \frac{1}{(16\pi^2)^2}\left[\left(3-\frac{\pi^2}{3s\sigma^2}\right)f + \frac{1}{2\sigma^2}f^2 - \frac{1}{3s\sigma^4}f^3 + 6 + \frac{\pi^2}{6}\right]$$

with

$$f = \sigma\ln\frac{1-\sigma}{1+\sigma} + i\pi\sigma.$$

In the notation of Ref. [10], this is

$$\overline{V}_1(s) = \frac{3}{N}\bar{J}(s) + \frac{K_1(s)}{2} - \frac{K_3(s)}{3} \ .$$

Of course, exactly the same method can be applied to integrals with a more complicated numerator.

A.3 The sunset diagram

For the sunset diagram integrals of the type

$$(H;H^\mu;H^{\mu\nu}) = \left\langle\left\langle \frac{(1;l_1^\mu;l_1^\mu l_1^\nu)}{[1-l_1^2][1-l_2^2][1-(p-l_1-l_2)^2]}\right\rangle\right\rangle \tag{A.9}$$

have to be calculated. Here we again focus on the scalar integral H, the remaining ones can be done analogously. For H we also present the procedure for the infinite part. Using the d-dimensional dispersion representation (A.2) for J, we get

$$H = \int_4^\infty [ds'] \int_0^1 dx \left\langle \frac{1}{[x + s'(1-x) - p^2 x(1-x) - l_1^2]^2} \right\rangle .$$

The $d^d l_1$ integrals can be performed easily and the result is

$$H(p^2) = \int_4^\infty [ds'] \int_0^1 dx \, F_2[z_2] \tag{A.10}$$

where

$$\begin{aligned} F_2[z_2] &= \frac{\Gamma(-\omega)}{(4\pi)^{2+\omega}} \, z_2^\omega \ , \\ z_2(p^2) &= x + s'(1-x) - p^2 x(1-x). \end{aligned} \tag{A.11}$$

We subtract and add the two first terms of the Taylor series of $F_2[z_2]$ in p^2 around $p^2 = 1$ and obtain for the finite part at $d = 4$

$$H(p^2) - H(1) - (p^2-1)H'(1) = \int_4^\infty ds' \sqrt{1 - \frac{4}{s'}} \int_0^1 dx \, \mathcal{K}_2(s', x; p^2),$$

where we have introduced the kernel

$$\begin{aligned} \mathcal{K}_2(s', x; p^2) &= \frac{1}{16\pi^2} \lim_{w \to 0} \Big\{ F_2[z_2(p^2)] - F_2[z_2(1)] - (p^2-1) F_2'[z_2(1)] \Big\} \\ &= -\frac{1}{(16\pi^2)^2} \left\{ \ln \frac{z_2(p^2)}{z_2(1)} + \frac{(p^2-1)x(1-x)}{z_2(1)} \right\}. \end{aligned}$$

The integral $\int dx \, \mathcal{K}_2$ could further be done in closed form – the result amounts to a twice subtracted one–loop self–energy integral with two propagators (with masses 1 and s'). In the text, we use

$$\overline{\overline{H}}(p^2) = \frac{1}{(p^2-1)^2} \int_4^\infty ds' \sqrt{1 - \frac{4}{s'}} \int_0^1 dx \, \mathcal{K}_2(s', x; p^2) \ , \tag{A.12}$$

which is finite at $p^2 = 1$. We also need $H(1)$ and $H'(1)$, where the poles at $\omega = 0$ are contained. For the evaluation of the infinite parts a recursion relation can be set up by partial integration in x in (A.10). This method gives [48]

$$\begin{aligned} H(1) &= -\frac{1}{(4\pi)^{4+2\omega}} \Gamma^2(-\omega) \left\{ \frac{3}{2} - \frac{17}{4}\omega + \frac{59}{8}\omega^2 + O(\omega^3) \right\} \ , \\ H'(1) &= -\frac{2}{(4\pi)^{4+2\omega}} \Gamma^2(-\omega) \left\{ \frac{1}{8}\omega + \frac{3}{16}\omega^2 + O(\omega^3) \right\}. \end{aligned} \tag{A.13}$$

In Ref. [49], the evaluation of the sunset integral is discussed in the general mass case.

B Off–shell four–point function in d dimensions

We display the four–point function to one loop in d dimensions. More precisely, we use the sigma model parametrization (3.3) and define

$$\begin{aligned} & i^3 \int dx_1\, dx_2\, dx_3\, e^{-i(p_1x_1+p_2x_2-p_3x_3-p_4x_4)} \langle 0|T\phi^i(x_1)\phi^k(x_2)\phi^l(x_3)\phi^m(x_4)|0\rangle \\ & = \frac{Z^2}{\prod_i (M_\pi^2 - p_i^2)} T^{lm;ik}(s,t,u;p_1^2,p_2^2,p_3^2,p_4^2) \end{aligned}$$

with[8]

$$\begin{aligned} & p_1 + p_2 = p_3 + p_4 \ , \\ & s = (p_1+p_2)^2 \ , \ t = (p_1-p_3)^2 \ , \ u = (p_1-p_4)^2 \ . \end{aligned}$$

The wave function renormalization constant Z is the one appearing in the two–point function (4.2). In the standard isospin decomposition

$$T^{lm;ik}(s,t,u;p_1^2,p_2^2,p_3^2,p_4^2) = \delta^{ik}\delta^{lm} A(s,t,u;p_1^2,p_2^2,p_3^2,p_4^2) + \text{ cycl. } ,$$

the scattering amplitude is obtained by putting all momenta on the mass shell,

$$A(s,t,u) = A(s,t,u;M_\pi^2,M_\pi^2,M_\pi^2,M_\pi^2) = \frac{s-M^2}{F^2} + O(p^4) \ .$$

We find

$$\begin{aligned} F^4 A(s,t,u;p_1^2,p_2^2,p_3^2,p_4^2) \ = \ & \\ & (s-M^2)\left\{F^2 + (2s+t+u-3M^2)J_1(s)\right\} \\ & + \left\{\left[p_1^2p_4^2 + p_2^2p_3^2 - t(p_2^2+p_3^2-t)\right] J_1(t) \right. \\ & + \left[\triangle_{13}\triangle_{24} - t(\triangle_{13}-\triangle_{24}+t)\right] J_2(t) \\ & \left. -2t\left[p_1^2+p_4^2-u\right] J_3(t) + (p_3,p_4,t) \to (p_4,p_3,u)\right\} \\ & + 8l_1 p_1p_2 \cdot p_3p_4 + 4l_2\left[p_1p_3 \cdot p_2p_4 + p_1p_4 \cdot p_2p_3\right] \\ & + \left[s + p_2^2 - p_1^2 - 5M^2/2\right] T_M \ , \end{aligned} \tag{B.1}$$

where

$$\begin{aligned} J_1(s) \ &= \ \frac{1}{2}J(s) \ , \ J_2(s) = -\frac{1}{s(d-1)}\left[\left(M^2 - \frac{d}{4}s\right)J(s) + \left(\frac{d}{2}-1\right)T_M\right] \ , \\ J_3(s) \ &= \ \frac{1}{s(d-1)}\left[\left(M^2 - \frac{s}{4}\right)J(s) - \frac{1}{2}T_M\right] \ \text{ and } \ \triangle_{ik} = p_i^2 - p_k^2 \ . \end{aligned} \tag{B.2}$$

Remarks:

[8] In Sect. 4, we express the Mandelstam variables in units of the physical pion mass squared. For simplicity of notation, we use in this appendix the standard definition.

i) For on–shell momenta, the result agrees at $d = 4$ with the result given in [2].

ii) For off–shell pions, the amplitude is not finite at $d = 4$, in contrast to the off–shell amplitude considered in [2], where the four–point function of pseudoscalar densities was considered. In that case, there are additional contributions proportional to the low–energy constants l_3 and l_4 that remove the remaining divergences.

iii) It is not surprising that the above amplitude is not finite off–shell: The construction given in Ref. [2] only guarantees that the Green functions built from quark currents are ultraviolet finite – Green functions of pion fields are unphysical objects, even if they occur at intermediate steps of a calculation, as in the present context.

iv) Finally, we mention that these divergences in the off–shell amplitude do not generate nonlocal singularities in the two–loop calculation.

C Scattering lengths and effective ranges

From the explicit expression for the scattering amplitude in equation (4.15), it is straightforward to evaluate the threshold parameters a_l^I and b_l^I. Using the definition (5.15), we find

$$\begin{aligned} a_0^0 &= \frac{7M_\pi^2}{32\pi F_\pi^2}\left\{1+\frac{x}{7}\left[49+5\,\bar{l}_1+12\,\bar{l}_2+48\,\bar{l}_3+32\,\bar{l}_4\right]\right. \\ &\quad \left.+x^2\left[\frac{7045}{63}-\frac{215\pi^2}{126}+10\,\bar{l}_1+24\,\bar{l}_2+96\,\bar{l}_3+64\,\bar{l}_4+\frac{192}{7}\,\bar{l}_5\right]\right\}\ , \end{aligned}$$

$$\begin{aligned} b_0^0 &= \frac{1}{4\pi F_\pi^2}\left\{1+\frac{x}{4}\left[\frac{281}{9}+4\,\bar{l}_2+48(\,\bar{l}_3+\,\bar{l}_4)\right]\right. \\ &\quad \left.+\frac{x^2}{4}\left[\frac{77489}{81}-\frac{4135\pi^2}{72}+\frac{10}{3}\,\bar{l}_1+\frac{592}{9}\,\bar{l}_2+\frac{6448}{9}\,\bar{l}_3+688\,\bar{l}_4+288\,\bar{l}_5-32\,\bar{l}_6\right]\right\}\ , \end{aligned}$$

$$a_0^2 = -\frac{M_\pi^2}{16\pi F_\pi^2}\left\{1-x\left[2+\,\bar{l}_1+16\,\bar{l}_4\right]+x^2\left[\frac{262}{9}-\frac{22\pi^2}{9}+4\,\bar{l}_1+64\,\bar{l}_4\right]\right\}\ ,$$

$$\begin{aligned} b_0^2 &= -\frac{1}{8\pi F_\pi^2}\left\{1-\frac{x}{2}\left[\frac{97}{18}-2\,\bar{l}_2+48\,\bar{l}_4\right]\right. \\ &\quad \left.+\frac{x^2}{2}\left[\frac{10591}{81}-\frac{145\pi^2}{12}+\frac{11}{3}\,\bar{l}_1-\frac{64}{9}\,\bar{l}_2+\frac{32}{9}\,\bar{l}_3+\frac{752}{3}\,\bar{l}_4+32\,\bar{l}_6\right]\right\}\ , \end{aligned}$$

$$
\begin{aligned}
a_1^1 &= \frac{1}{24\pi F_\pi^2}\left\{1 + x\left[-\frac{17}{36} + \bar{l}_2 + 8\,\bar{l}_4\right]\right. \\
&\quad \left. + x^2\left[-\frac{181}{162} + \frac{7\pi^2}{24} - \frac{5}{6}\,\bar{l}_1 - \frac{16}{9}\,\bar{l}_2 - \frac{16}{3}\,\bar{l}_3 - \frac{8}{3}\,\bar{l}_4 + 16\,\bar{l}_6\right]\right\} \quad , \\
b_1^1 &= \frac{1}{256\pi^3 F_\pi^4}\left\{\frac{37}{135} - \frac{8}{3}\,\bar{l}_3 + 8\,\bar{l}_4 + \right. \\
&\quad \left. + x\left[\frac{56981}{2430} - \frac{337\pi^2}{810} - 2\,\bar{l}_1 - \frac{196}{135}\,\bar{l}_2 - \frac{1888}{135}\,\bar{l}_3 - \frac{544}{135}\,\bar{l}_4 + \frac{64}{3}\,\bar{l}_6\right]\right\} \quad , \\
a_2^0 &= \frac{1}{480\pi^3 F_\pi^4}\left\{-\frac{47}{72} + \bar{l}_3 + 7\,\bar{l}_4\right. \\
&\quad \left. + x\left[\frac{7003}{2160} + \frac{169\pi^2}{2160} + \frac{1}{12}\,\bar{l}_1 - \frac{11}{9}\,\bar{l}_2 - \frac{152}{45}\,\bar{l}_3 - \frac{364}{45}\,\bar{l}_4 + 32\,\bar{l}_6\right]\right\} \quad , \\
a_2^2 &= \frac{1}{480\pi^3 F_\pi^4}\left\{-\frac{49}{360} + \bar{l}_3 + \bar{l}_4\right. \\
&\quad \left. + x\left[-\frac{67}{2160} - \frac{127\pi^2}{432} + \frac{29}{60}\,\bar{l}_1 + \frac{19}{90}\,\bar{l}_2 + \frac{28}{45}\,\bar{l}_3 + \frac{188}{45}\,\bar{l}_4 + 8\,\bar{l}_6\right]\right\} \quad ,
\end{aligned}
\tag{C.1}
$$

where

$$
x = \frac{M_\pi^2}{16\pi^2 F_\pi^2} \quad , \quad \bar{l}_{1,2,3,4} = 16\pi^2 l_{1,2,3,4} \ \text{ and } \ \bar{l}_{5,6} = (16\pi^2)^2 l_{5,6} \ . \tag{C.2}
$$

The coefficients l_i are displayed in appendix D. The terms between the last square brackets in the expressions for a_l^I and b_l^I generate contributions of $O(p^8)$ – these are beyond the accuracy we aim at here. In order to keep the formulae as simple as possible, we nevertheless retain them. In our numerical results these are removed.

D The constants l_i

The quantities l_i in Eqs. (4.14) and (4.15) stand for

$$
\begin{aligned}
l_1 &= 8\,l_1^r + 2\,l_3^r - 2\,l_4^r + \frac{7}{6}L + \frac{1}{16\pi^2}\frac{13}{18} \\
&+ x_2\left\{\frac{1}{16\pi^2}\left[\frac{56}{9}\,l_1^r + \frac{80}{9}\,l_2^r + 15\,l_3^r + \frac{26}{9}\,l_4^r + \frac{47}{108}L - \frac{17}{216} + \frac{1}{16\pi^2}\frac{3509}{1296}\right]\right.
\end{aligned}
$$

$$+\frac{1}{6}\left[4k_1+28k_2-6k_3+13k_4\right]+\left[32\,l_1^r+12\,l_3^r-5\,l_4^r\right]\,l_4^r-8\,{l_3^r}^2+r_1^r\Big\}\ ,$$

$$\begin{aligned}
b_2 &= -8\,l_1^r+2\,l_4^r-\frac{2}{3}L-\frac{1}{16\pi^2}\frac{2}{9}\\
&+ x_2\Big\{\frac{1}{16\pi^2}\Big[-24\,l_1^r-\frac{166}{9}\,l_2^r-18\,l_3^r-\frac{8}{9}\,l_4^r-\frac{203}{54}L+\frac{317}{3456}-\frac{1}{16\pi^2}\frac{1789}{432}\Big]\\
&\qquad -\frac{1}{6}\left[54k_1+62k_2+15k_3+10k_4\right]-\left[32\,l_1^r+4\,l_3^r-5\,l_4^r\right]\,l_4^r+r_2^r\Big\}\ ,\\
b_3 &= 2\,l_1^r+\frac{1}{2}\,l_2^r-\frac{1}{2}L-\frac{1}{16\pi^2}\frac{7}{12}+x_2\Big\{\frac{1}{16\pi^2}\Big[\frac{178}{9}\,l_1^r+\frac{38}{3}\,l_2^r-\frac{7}{3}\,l_4^r-\frac{365}{216}L\\
&\qquad -\frac{311}{6912}+\frac{1}{16\pi^2}\frac{7063}{864}\Big]+2\left[4\,l_1^r+\,l_2^r\right]\,l_4^r+\frac{1}{6}\left[38k_1+30k_2-3k_4\right]+r_3^r\Big\}\ ,\\
b_4 &= \frac{1}{2}\,l_2^r-\frac{1}{6}L-\frac{1}{16\pi^2}\frac{5}{36}+x_2\Big\{\frac{1}{16\pi^2}\Big[\frac{10}{9}\,l_1^r+\frac{4}{9}\,l_2^r-\frac{5}{9}\,l_4^r+\frac{47}{216}L\\
&\qquad +\frac{17}{3456}+\frac{1}{16\pi^2}\frac{1655}{2592}\Big]+2\,l_2^r\,l_4^r-\frac{1}{6}\left[k_1+4k_2+k_4\right]+r_4^r\Big\}\ ,\\
b_5 &= \frac{1}{16\pi^2}\Big[-\frac{31}{6}\,l_1^r-\frac{145}{36}\,l_2^r+\frac{625}{288}L+\frac{7}{864}-\frac{1}{16\pi^2}\frac{66029}{20736}\Big]-\frac{21}{16}k_1-\frac{107}{96}k_2+r_5^r\ ,
\end{aligned}$$

$$b_6 = \frac{1}{16\pi^2}\Big[-\frac{7}{18}\,l_1^r-\frac{35}{36}\,l_2^r+\frac{257}{864}L+\frac{1}{432}-\frac{1}{16\pi^2}\frac{11375}{20736}\Big]-\frac{5}{48}k_1-\frac{25}{96}k_2+r_6^r\ , \tag{D.1}$$

where

$$\begin{aligned}
L &= \frac{1}{16\pi^2}\ln\frac{M_\pi^2}{\mu^2}\ ,\\
k_i &= (4\,l_i^r(\mu)-\gamma_i L)L\ ;\ \gamma_1=\frac{1}{3}\ ,\ \gamma_2=\frac{2}{3}\ ,\ \gamma_3=-\frac{1}{2}\ ,\ \gamma_4=2\ .
\end{aligned} \tag{D.2}$$

We have denoted by l_i^r (r_i^r) the renormalized, quark mass independent couplings from $\mathcal{L}_4$ ($\mathcal{L}_6$), with [2] $\mu\dfrac{dl_i^r}{d\mu}=-\dfrac{\gamma_i}{16\pi^2}$. In the text, we also use the parameters $\bar{l}_i$, defined by

$$l_i^r=\frac{\gamma_i}{32\pi^2}\left(\bar{l}_i+\ln\frac{M_\pi^2}{\mu^2}\right)\ . \tag{D.3}$$

The scale dependence of r_i^r is fixed by the requirement $\mu\dfrac{db_i}{d\mu}=0$.

References

[1] S. Weinberg, Physica 96A (1979) 327.

[2] J. Gasser and H. Leutwyler, Ann. Phys. (N.Y.) 158 (1984) 142.

[3] J. Gasser and H. Leutwyler, Nucl. Phys. B 250 (1985) 465.

[4] H. Leutwyler, Ann. Phys. (N.Y.) 235 (1994) 165.

[5] S. Weinberg, Phys. Rev. Lett. 17 (1966) 616.

[6] J. Gasser and H. Leutwyler, Phys. Lett. B 125 (1983) 325.

[7] L. Maiani, G. Pancheri and N. Paver (eds.), The Second DAΦNE Physics Handbook (INFN, Frascati, 1995).

[8] A.M. Bernstein and B.R. Holstein (eds.), Chiral Dynamics: Theory and Experiment, Proceedings of the Workshop held at MIT, Cambridge, MA, USA, 25–29 July 1994 (Springer, Berlin and Heidelberg, 1995).

[9] M. Knecht, B. Moussallam, J. Stern and N.H. Fuchs, Nucl. Phys. B 457 (1995) 513.

[10] J. Bijnens, G. Colangelo, G. Ecker, J. Gasser and M.E. Sainio, Phys. Lett. B 374 (1996) 210.

[11] G. Wanders, Univ. Lausanne preprint, hep-ph/9705323.

[12] G. Wanders, Helv. Phys. Acta 70 (1997) 287.

[13] B. Ananthanarayan, D. Toublan and G. Wanders, Phys. Rev. D 51 (1995) 1093; Phys. Rev. D 53 (1996) 2362.

[14] D. Toublan, Phys. Rev. D 53 (1996) 6602.

[15] J. Sá Borges, J. Soares Barbosa and V. Oguri, Phys. Lett. B 393 (1997) 413.

[16] B. Ananthanarayan and P. Büttiker, Phys. Rev. D 54 (1996) 1125; Phys. Rev. D 54 (1996) 5501.

[17] M.R. Pennington and J. Portolés, Phys. Lett. B 344 (1995) 399; Phys. Rev. D 55 (1997) 3082.

[18] M. Knecht, B. Moussallam, J. Stern and N.H. Fuchs, Nucl. Phys. B 471 (1996) 445.

[19] G. Colangelo, Phys. Lett. B 350 (1995) 85; Phys. Lett. B 361 (1995) 234 (E).

[20] L. Girlanda, M. Knecht, B. Moussallam and J. Stern, preprint IPNO/TH 97-08, CPT-97/P.3470, hep-ph/9703448.

[21] J. Bijnens, G. Colangelo and J. Gasser, Nucl. Phys. B 427 (1994) 427.

[22] I. Jack and H. Osborn, Nucl. Phys. B 207 (1982) 474.

[23] S. Bellucci, J. Gasser and M.E. Sainio, Nucl. Phys. B 423 (1994) 80; Nucl. Phys. B 431 (1994) 413 (E).

[24] U. Bürgi, Phys. Lett. B 377 (1996) 147; Nucl. Phys. B 479 (1996) 392.

[25] J.A.M. Vermaseren, Symbolic Manipulation with FORM: tutorial and reference manual, version 2 (Computer Algebra Nederland, Amsterdam, 1991).

[26] H.W. Fearing and S. Scherer, Phys. Rev. D 53 (1996) 315.

[27] J. Bijnens et al., in preparation.

[28] J.C. Collins, Renormalization (Cambridge University Press, Cambridge, 1984).

[29] W.A. Bardeen, A.J. Buras, D.W. Duke and T. Muta, Phys. Rev. D 18 (1978) 3998.

[30] D. Bessis and M. Pusterla, Nuovo Cim. A54 (1968) 243.

[31] G. Ecker and M. Mojžiš, Phys. Lett. B 365 (1996) 312.

[32] N.H. Fuchs, H. Sazdjian and J. Stern, Phys. Lett. B 269 (1991) 183;
J. Stern, H. Sazdjian and N.H. Fuchs, Phys. Rev. D 47 (1993) 3814;
M. Knecht and J. Stern, in Ref. [7], p. 169.

[33] J. Bijnens and P. Talavera, Nucl. Phys. B 489 (1997) 387.

[34] G. Colangelo, Phys. Lett. B 395 (1997) 289;
G. Colangelo and E. Pallante, Pion loops in quenched Quantum Chromodynamics, BUTP–97/06 (hep–lat/9702019).

[35] G. Ecker, J. Gasser, A. Pich and E. de Rafael, Nucl. Phys. B 321 (1989) 311.

[36] G. Ecker, J. Gasser, H. Leutwyler, A. Pich and E. de Rafael, Phys. Lett. B 223 (1989) 425.

[37] G. Ecker, A. Pich and E. de Rafael, Phys. Lett. B 237 (1990) 481;
P. Ko, Phys. Rev. D 41 (1990) 1531;
J. Bijnens, S. Dawson and G. Valencia, Phys. Rev. D 44 (1991) 3555.

[38] M. Praszalowicz and G. Valencia, Nucl. Phys. B 341 (1990) 27;
A.A. Bel'kov, A.V. Lanyov, A. Schaale and S. Scherer, Acta Phys. Slovaca 45 (1995) 121;
M.V. Polyakov and V.V. Vereshagin, Phys. Rev. D 54 (1996) 1112.

[39] J. Gasser, M.E. Sainio and A. Švarc, Nucl. Phys. B 307 (1988) 779.

[40] O. Dumbrajs et al., Nucl. Phys. B 216 (1983) 277.

[41] H. Leutwyler et al., work in progress.

[42] L. Rosselet et al., Phys. Rev. D 15 (1977) 574.

[43] W. Hoogland et al., Nucl. Phys. B 126 (1977) 109.

[44] M.L. Goldberger and K.M. Watson, Collision Theory (John Wiley, New York, 1964).

[45] J.L. Basdevant, C.D. Froggatt and J.L. Petersen, Nucl. Phys. B 72 (1974) 413.

[46] B. Adeva et al., *Lifetime measurement of $\pi^+\pi^-$–atoms to test low energy QCD predictions*, Proposal to the SPSLC, CERN/SPSLC 95-1, SPSLC/P 284, Geneva 1995.

[47] N. Nakanishi, Graph theory and Feynman integrals (Gordon and Breach, New York and London, 1971).

[48] U. Bürgi et al., in preparation.

[49] P. Post and J.B. Tausk, Mod. Phys. Lett. A11 (1996) 2115.